HAL
open science

Palaeosecular variation recorded by 9 ka to 2.5-Ma-old lavas from Martinique Island: new evidence for the La Palma aborted reversal ∼617 ka ago

Cyrielle Tanty, Julie Carlut, Jean-Pierre Valet, Aurélie Germa

▶ To cite this version:

Cyrielle Tanty, Julie Carlut, Jean-Pierre Valet, Aurélie Germa. Palaeosecular variation recorded by 9 ka to 2.5-Ma-old lavas from Martinique Island: new evidence for the La Palma aborted reversal ∼617 ka ago. Geophysical Journal International, 2015, 200, pp.917-934. 10.1093/gji/ggu423 . insu-03580028

HAL Id: insu-03580028

https://insu.hal.science/insu-03580028v1

Submitted on 6 Sep 2022

HAL is a multi-disciplinary open access archive for the deposit and dissemination of scientific research documents, whether they are published or not. The documents may come from teaching and research institutions in France or abroad, or from public or private research centers.

L'archive ouverte pluridisciplinaire **HAL**, est destinée au dépôt et à la diffusion de documents scientifiques de niveau recherche, publiés ou non, émanant des établissements d'enseignement et de recherche français ou étrangers, des laboratoires publics ou privés.

Geophysical Journal International

Geophys. J. Int. (2015) **200,** 917–934 doi: 10.1093/gji/ggu423

GJI Geomagnetism, rock magnetism and palaeomagnetism

Palaeosecular variation recorded by 9 ka to 2.5-Ma-old lavas from Martinique Island: new evidence for the La Palma aborted reversal ∼617 ka ago

Cyrielle Tanty,[1] Julie Carlut,[1] Jean-Pierre Valet[1] and Aurélie Germa[2]

[1]*Institut de Physique du Globe de Paris, Université Paris Diderot, Sorbonne Paris Cité, UMR* 7154 *CNRS, 1 rue Jussieu, F-*75238 *Paris Cedex* 05*, France. E-mail: carlut@ipgp.fr*

[2]*School of Geosciences, University of South Florida, Tampa, FL* 33620*, USA*

Accepted 2014 October 28. Received 2014 October 28; in original form 2014 May 7

SUMMARY

Fifteen sites of lava flows from Martinique Island (FWI) have been selected to document the geomagnetic field in the Caribbean area over the past 2.5 Ma and further constrain the time-averaged field during this period. Identical characteristic directions were isolated using both AF and thermal stepwise demagnetization techniques in all flows. Nine mean-site directions have a normal polarity, while three others are reversed. The mean geomagnetic pole position obtained after reducing all directions to the same polarity is indistinguishable from the present north geographic pole. The dispersion is at least 8° larger than the values derived from the time-averaged field models and remains unexplained otherwise than resulting from the relatively small number of directions. The other three flows are characterized by large deviations from the expected north–south direction. One lava flow dated at 1.69 Ma (±0.02 Ma) is likely associated with a transitional field during the Gilsà subchron. The lava flow dated at 770 ka (±11 ka) coincides with the age of the Brunhes-Matuyama geomagnetic reversal and is also coeval with another intermediate flow of the same age found at Guadeloupe Island. The 617 ka (±52 ka) old unit is characterized by reversed directions that are evidently not related to the last reversal, but with other reversed polarity and transitional lava flows of the same age recorded, respectively at Mexico and La Palma island. We infer that the presence of reversed directions with the same age at distinct localities confirms that a short episode of reversed polarity has occurred during this period.

Key words: Geomagnetic excursions; Magnetic field; Magnetic mineralogy and petrology; Magnetostratigraphy; Palaeomagnetic secular variation; Reversals: process, time scale, magnetostratigraphy.

1 INTRODUCTION

During the past decade, multiple studies were conducted to obtain high quality palaeomagnetic records from lava flows that document the variability of the Earth's magnetic field beyond the historical and archeological periods (Tauxe *et al.* 2003; Elmaleh *et al.* 2004; Mejia *et al.* 2004, 2005; Tauxe *et al.* 2004; Opdyke *et al.* 2006; Johnson *et al.* 2008; Brown *et al.* 2009; Quidelleur *et al.* 2009). A large part of this effort was devoted at resolving second-order persistent non-dipolar patterns in the time averaged geomagnetic field (TAF). Although the hypothesis of a geocentred axial dipole has been extensively used by palaeomagnetists, it has been suggested for some time that the TAF is best modelled with the additional contribution of a small axial quadrupole (Wilson 1970; Merrill & McElhinny 1977; Constable & Parker 1988; Schneider & Kent 1990; Quidelleur *et al.* 1994; Carlut & Courtillot 1998; Johnson *et al.* 2008). A challenging observation derived from recent data sets is that the Brunhes and Matuyama chrons would be characterized by different TAF geometries (Johnson *et al.* 2008), thereby suggesting that the Earth's magnetic field has specific statistical characteristics for different time periods. Large persistent deviations from the local dipole field direction have also been reported at several localities for time periods of a few tens of ka (Zanella 1998; Elmaleh *et al.* 2001, 2004). Whether these local features have any global significance remains to be demonstrated, and would represent a significant step towards a comprehensive description of the field variability.

Carlut *et al.* (2000) contributed to the study of the time-averaged field by studying 0–1-Ma-old lava flows from Guadeloupe Island (eastern Caribbean area). They found different mean directions for the 700–400 ka and the 400–0 ka periods and suggested to use subdata sets within these time intervals to compute TAF models for the Caribbean area. Furthermore, the results provided a number of testable hypotheses for the TAF. With these results in mind, we decided to contribute further by focusing on the close by Martinique Island. Recent studies (Samper *et al.* 2008; Germa *et al.*

© The Authors 2014. Published by Oxford University Press on behalf of The Royal Astronomical Society.

Downloaded from http://gji.oxfordjournals.org/ at Erciyes University on December 21, 2014

2010; Germa *et al.* 2011) have improved our knowledge of the volcanic history of Martinique Island which is now documented by a set of K–Ar ages. A large number of flows were found with ages within the Brunhes and Matuyama Chrons (i.e. the past 2.5 Myr) and were thus very appropriate to search for anomalous directions that would indicate a deviation of the field from the local dipolar direction. In addition, volcanic records obtained during the past years have confirmed the presence of large deviations of the geomagnetic field away from the normal range of secular variation, but they remain very limited because such short events are difficult to capture within the short time window of a volcanic eruption (Roberts 2008; Singer *et al.* 2008). It is unclear whether these excursions and/or rapid events that are usually accompanied by low intensities must be regarded as large episodes of secular variation or as aborted geomagnetic reversals. Detailed knowledge of their frequency and spatial occurrence is of crucial importance as it imposes strong constraints to the dynamo models (Gubbins 1999; Valet *et al.* 2008). In order to meet these objectives, a sampling trip was conducted in the Martinique Island in 2012 to perform a palaeomagnetic and exhaustive sampling of these new dated flows.

2 GEOLOGICAL SETTINGS AND PALAEOMAGNETIC SAMPLING

The Lesser Antilles Island arc results from the subduction of the Atlantic Plate under the Caribbean Plate and is composed of three distinct volcanic branches. The ages of the old, intermediate and recent arcs, respectively from east to west, range from Late Oligocene to present (Briden *et al.* 1979; Westercamp *et al.* 1989). The Martinique Island is located in the central part of the Lesser Antilles arc and was built from several volcanic complexes (Fig. 1). Volcanic activity progressively migrated westward and the edifices belonging to the most recent arc are found in the Northern and Western parts of the island (Westercamp *et al.* 1989). New K–Ar ages reported by Germa *et al.* (2010, 2011) constrain the eruptive history of the five distinct volcanic centres that compose the recent arc (Fig. 1). It is now established that Morne Jacob volcano was active between about 5.2 and 1.5 Ma. Trois Ilets and Carbet Complexes started being active at, respectively 2.3 and 1 Ma, activity ended ∼0.3 Ma. Mount Conil erupted between ∼550 and ∼125 ka, and the still active Montagne Pelée is younger than 125 ka.

Palaeomagnetic sampling took place in 2012 February and was focused on the lava flows dated by Germa *et al.* (2010, 2011) and Samper *et al.* (2008). We restrained the sampling to the five most recent volcanic centres: Morne Jacob, Trois Ilets, Carbet Complex, Mount Conil and Montagne Pelée (Fig. 1) and we selected flows belonging to the Brunhes and Matuyama chron (i.e. younger than 2.5 Ma). Outcrops were mostly located along road or path cuts and in stream beds. Stratigraphy was often difficult to follow due to the dense vegetal covers however no evidence for tilting was observed. Cores were sampled over several meters to several tens of metres along the outcrops. An average of 9–10 cores were drilled at each site reaching a total of 218 palaeomagnetic cores corresponding to 23 independent flows (Fig. 1). Four flows were located on Conil, 2 on Montagne Pelée, 3 on the Trois Ilet, 5 on Morne Jacob and 9 on Carbet complex (Fig. 1 and Table 1).

Sun compass was systematically preferred to magnetic orientation when atmospheric conditions and vegetal cover were favourable. Magnetic declination was usually found within 2° from the expected International Geomagnetic Reference Field (IGRF) value at Martinique Island (−14.8° in 2012). A mean magnetic declination of −14.9° ± 1.8° was derived from the 18 sites with sun orientation and testifies to the absence of large geomagnetic anomaly over the spatial scale of a sampling site. Whenever sun compass orientations could not be performed (six sites), the mean magnetic declination was used to correct for magnetic orientation.

3 LABORATORY TREATMENT

A total of 190 samples were demagnetized and measured in the magnetic shielded room at IPG-Paris. Three to nine specimens from each flow were stepwise thermally demagnetized, while two to five specimens were stepwise demagnetized by alternating fields (AF). The natural remanent magnetization (NRM) was measured using an Agico JR-5 spinner magnetometer. A 2G cryogenic magnetometer was also used for a few samples. Thermal demagnetization was performed at 15–16 temperature steps (every 40 °C from 120 to 440 and then every 20 °C to 540 and two steps at 555 and 570 °C) until remanence is less than 2 per cent of its initial value. Additional heating at 600, 615, 630 and 645 °C was performed for a few samples. Eleven steps have been used for AF demagnetization (5, 8, 12, 16, 20, 25, 30, 40, 60, 80 and 100 mT). In addition, a batch of samples was subjected to continuous thermal demagnetization using a Triaxe vibrating sample magnetometer at IPG-Paris (Le Goff & Gallet 2004). Continuous measurements and fast heating to high temperatures allow to monitor the spontaneous magnetization and to track anomalous behaviour of the remanence (Plenier *et al.* 2007; Coe *et al.* 2014). The samples were demagnetized in a 5 mT field prior to the measurements in order to cancel out the softer viscous components and their three axes magnetic moments were continuously documented during heating and cooling at a rate of ∼30 °C min^{-1} in zero field.

Low-field thermomagnetic susceptibility measurements [$\kappa(T)$] were performed on 1 cm^3 samples powders from each site using an Agico KLY-3 equipped with a CS-3 at IPG-Paris. Heating-cooling runs were performed in air from 20 up to 620 or 650 °C. Hysteresis loops and high resolution IRM acquisition curves were obtained for a representative sample from all sites using an alternating gradient magnetometer (AGFM, Princeton Measurements Corporation) at IPGP. The acquisition curves of isothermal remanent magnetization (IRM) were unmixed using the CLG function (Kruiver *et al.* 2001) in order to isolate magnetic components with different coercivities.

Finally, microscopic observations and semi-quantitative chemical data were collected on five thin sections from sites MTAA, MTAC, MT06, MT38 and MT57 using a field emission scanning electronic microscope (Fe-SEM, Zeiss Sigma) equipped with an EDS detector (Oxford instrument) at École Normale Supérieure de Paris (ENS, Paris).

4 RESULTS

4.1 Demagnetization behaviour

Results are shown in Figs 2 and 3. Most samples were totally demagnetized (i.e. with more than 95 per cent of the NRM is lost) after experiencing a 80 mT AF or being heating in zero field at 555–570 °C (Fig. 2). The characteristics suggest that fine grained Ti-poor magnetite is the main carrier of the remanence. For a few samples (from sites from sites MTAC, MTAA, MT16, MT38, MT48 and MT57) a small portion of NRM was resistant beyond 615 °C and sometimes up to 630 °C (Figs 2a and c). This phase carries less than 10 per cent of the initial remanence, except at site MTAC,

Downloaded from http://gji.oxfordjournals.org/ at Erciyes University on December 21, 2014

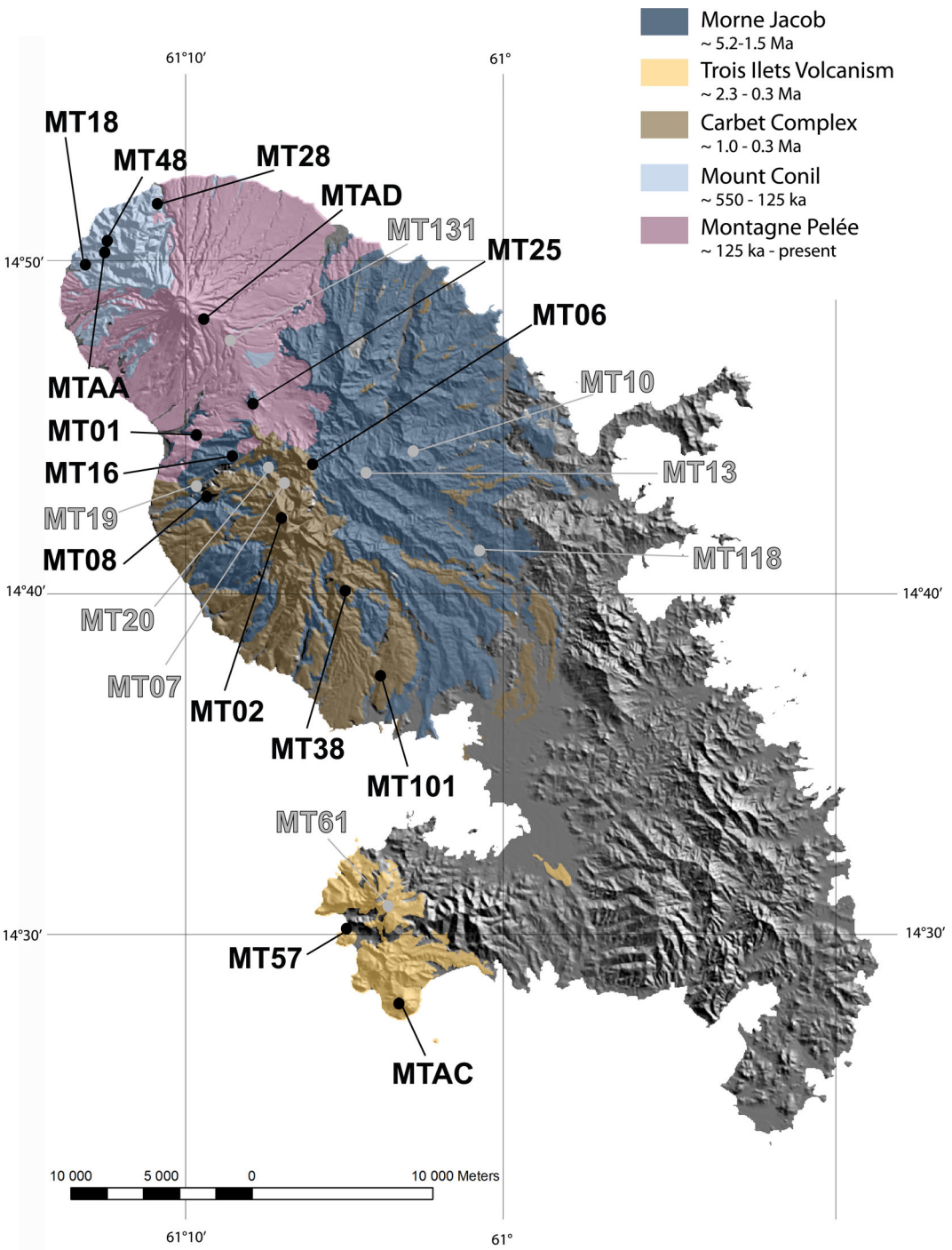

Figure 1. Sampling site locations. Schematic geological map of Martinique Island (Germa *et al.* 2010) showing the locations of the volcanic complexes and sampling sites. Sites in grey (resp. black) colours correspond to unsuccessful (resp. successful) palaeomagnetic determinations.

where it can represents up to 30 per cent of the initial signal. A few samples exhibited erratic directions during demagnetization so that no characteristic component could be isolated (Fig. 2f).

4.2 Thermomagnetic experiments

The characteristics of the thermomagnetic experiments contribute to refine these observations. All samples display a dominant ferromagnetic phase with a decrease in susceptibility within 550–580 °C and thus generated by the presence of Ti-poor magnetite. In addition a minor phase characterized by a decrease between 300 and 400 °C (Figs 4a and b) is sometimes present (e.g. for sites MT01, MT02, MT06, MT08, MT16, MT38, MT48 and MT57). Such behaviour likely reflects the contribution of cation deficient Ti-poor magnetite (with a typical destabilization temperature around 350 °C) or the occurrence of Ti-rich magnetite (with a range of Curie temperatures within 300–400 °C). In these samples the heating and cooling curves are not fully reversible due to destabilization of the Ti-rich

Downloaded from http://gji.oxfordjournals.org/ at Erciyes University on December 21, 2014

and/or cation deficient phase. Half of the samples (MT08, MT101, MT16, MT25, MT38, MT48 and MTAC in Fig. 4c) also show a tiny high temperature phase (less than 5 per cent from total susceptibility) which was removed at about 620 °C and is thus typical of substituted hematite. A specific behaviour has been observed for site MTAA with a sharp increase of magnetization beyond 120 °C (Fig. 4d) and two sharp drops at 300 and 550 °C. The shape of the thermomagnetic curve is very similar to that of ultramafic rocks (MacLeod *et al.* 2011), despite this peculiar behaviour possibly due to the alteration of an unknown phase an important fraction of the magnetization is carried by Ti-poor magnetite.

Altogether the thermomagnetic results and the characteristics inherent to the demagnetization diagrams (Figs 2 and 3) confirm that Ti-poor magnetite is the main magnetic carrier with the addition of minor Ti-rich magnetite and/or Ti-maghemite. In a few cases a small fraction of Ti-hematite is also present.

4.3 Directional analyses and site mean directions

The majority of specimens exhibited a simple directional behaviour after removal of a minor secondary viscous component vanishing after 160–200 °C or in a 8–12 mT AF (Figs 2a–c and e). The intra-site dispersion of the directions is low (see e.g. site MT57 in Figs 3e–h). A few specimens (specifically from site MT06) exhibited a more complex behaviour (Figs 2d and 3a–d and f) with a secondary component that was not removed before 320–440 °C or AF fields of 16–20 mT. At site MT06 its direction (Inc = 25.3; dec = −13.5; $\alpha_{95} = 6.8$ for $n = 9$) points towards the present local field (2012) (Inc = 37.3; dec = −14.8).

The characteristic direction was determined by principal component analysis (Kirschvink 1980) using the Palaeomac software (Cogné 2003). For a few specimens from sites MT06 and MT02, directions were obtained by the great circle technique (see Fig. 3c). Twenty specimens did not provide any readily interpretable palaeodirection and were thus rejected.

The mean palaeomagnetic direction for each site was obtained using the Fisher's statistics (Fisher 1953) or mixed statistics whenever great circles were used. The individual directions derived from sites MT07, MT10, MT13, MT19, MT20, MT61 and MT131 were inconsistent, and consequently we did not retain any mean-site direction from these sites. These inconsistencies were caused by a large number of displaced blocks, probably linked to the explosive nature of the volcanism and/or to flank collapses and landslides (Boudon *et al.* 2007, 2013; Aubaud *et al.* 2013) that make the area prone to mass movement of ground rocks. Field observations were indeed more delicate for these sites to detect tilting or motions of large blocks mostly because of dense vegetal cover. All other sites could be carefully checked and did not reveal any problem. A well-defined palaeomagnetic direction was thus isolated from 15 out of the 23 sites. Individual directions at each site with their associated mean site direction are shown in Fig. 5.

The site mean palaeomagnetic directions and their associated virtual geomagnetic poles (VGPs) are reported in Table 1 and directions are plotted in stereographic projection in Fig. 6. All sites but one have a precision parameter (k) above 50 and little intrasite scatter. Site MT06 with $k = 13.9$ exhibits a larger within site dispersion due to large secondary components which added noise to the data. Nine sites with a VGP position above 45° in the Northern hemisphere (Fig. 7) have a clear normal polarity, while five sites with mean inclinations lower than −45° are reverse. Site MT06 is characterized by the lowest VGP latitude (32.7°). Whether or not

Table 1. Palaeomagnetic results. Column headings indicate: site number, flow location, site latitude, site longitude, age in Ma (Germa *et al.* 2010, 2011; Samper *et al.* 2008), number of data used/total number of samples measured, Declination in degrees, Inclination in degrees), Fisher's precision parameter, radius of the 95 per cent confidence cone from Fisher 1953 statistics, VGP longitude), VGP latitude. Stars in the Age column indicate: (*) 12MTAC was labelled 06MT56 by Germa *et al.* 2011 and is identical to 06MT59 (**) age given for the site 12MTAA is the mean age of Mount Conil.

Site	Flow location		Site lat.	Site long.	Age (Ma)		n/N	Dec.	Inc.	k	α_{95}	VGP long.	VGP lat.
MT01	Bellevue	Carbet Complex	14.75	61.16	1.69 ± 0.02	Fisher	7/7	134.6	−51.4	255.8	3.8	59.6	−45.3
MT02	Carbet-Morne Piquet	Carbet Complex	14.71	61.12	0.331 ± 0.005	Mixte	9/12	2.0	−21.2	58.3	6.8	114.3	64.3
MT06	Piton Gelé	Carbet Complex	14.74	61.10	0.770 ± 0.011	Mixte	11/11	−56.3	1.6	13.9	12.7	200.2	32.7
MT08	Pt de la Campbeilh	Morne Jacob Shield Volcano	14.72	61.16	2.27 ± 0.03	Fisher	6/7	167.4	−39.9	138.4	5.7	64.5	−75.7
MT101	Ravine Vilaine	Morne Jacob Shield Volcano	14.62	61.07	1.81 ± 0.03	Fisher	8/8	−0.4	20.0	213.7	3.8	123.6	85.7
MT16	Morne des Cadets	Morne Jacob Shield Volcano	14.74	61.14	1.61 ± 0.02	Fisher	9/11	165.3	−51.6	107.3	5.0	83.9	−67.9
MT18	Morne du Céron	Conil Complex	14.84	61.22	0.346 ± 0.042	Fisher	6/8	38.6	19.4	105.7	6.5	31.5	52.1
MT25	Morne Balisier	Morne Jacob Shield Volcano	14.77	61.13	2.12 ± 0.03	Fisher	8/9	189.5	−23.8	236.4	3.6	222.1	−80.5
MT28	Grand'Rivière	Conil Complex	14.87	61.18	0.543 ± 0.008	Fisher	10/11	−28.2	38.3	92.8	5.0	227.0	62.5
MT38	Cascade Absalon	Morne Jacob Shield Volcano	14.68	61.09	1.86 ± 0.03	Fisher	6/8	−7.6	40.6	353.9	3.6	260.1	78.9
MT48	Morne à Lianes	Conil Complex	14.85	61.21	0.207 ± 0.003	Fisher	6/9	2.3	1.3	143.4	5.6	109.3	75.7
MT57	Morne Champagne	Trois Ilets Volcanism	14.50	61.09	0.617 ± 0.052	Fisher	7/8	172.2	−36.6	309.7	3.4	68.5	−80.5
MTAA	Morne à Lianes	Conil Complex	14.84	61.22	0.337 ± 0.213**	Fisher	7/8	24.9	21.9	176.4	4.6	33.8	65.5
MTAC	Morne Larcher	Trois Ilets Volcanism	14.46	61.06	0.346 ± 0.027*	Fisher	7/7	9.8	−5.6	467.2	2.8	88.8	70.2
MTAD	Aileron	Montagne Pelée	14.81	61.16	0.0097 ± 0.0005	Fisher	6/9	−5.5	38.4	203.5	4.7	262.3	81.4

Downloaded from http://gji.oxfordjournals.org/ at Erciyes University on December 21, 2014

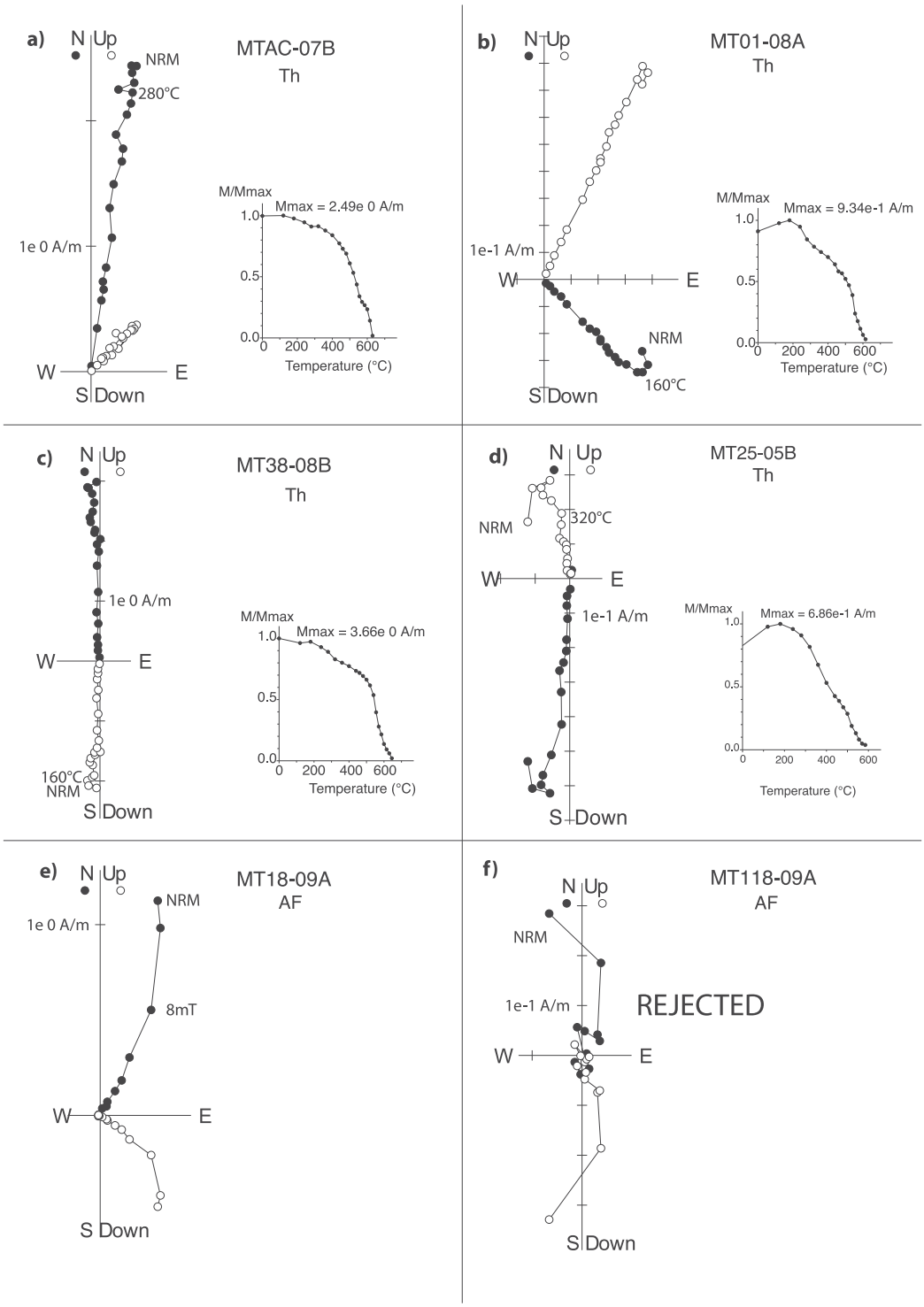

Figure 2. Demagnetization diagrams. (a–d) Thermal vector end-point diagrams of representative samples with simple behaviour after removing minor secondary components, (e) typical AF vector end-point diagrams of specimen with simple behaviour (f) example of rejected specimen due to complex behaviour during AF demagnetization. Solid symbols correspond to projections onto the horizontal plane, while open symbols represent projections onto the vertical plane. Insets show thermal demagnetization curves corresponding to Zijderveld diagrams, the magnetic moment is normalized to its maximum value.

this site must be seen as transitional depends on the amplitude of secular variation. The number of sites with normal and reverse polarity is insufficient for a full description of the secular variation in the area. We thus used a conservative approach based on the VGP cut-off angle of 45° (Watkins 1973). Based on these criteria, site MT06 is clearly transitional.

4.4 Reliability of the directions

Lava flows are considered as accurate recorders of the magnetic field. However, in some rare occasions magnetic coupling or undetected alteration during laboratory treatment can generate significant deviations from the original field direction (Krása *et al.* 2005; Plenier *et al.* 2007; Coe *et al.* 2014). Recently, demagnetization of

Downloaded from http://gji.oxfordjournals.org/ at Erciyes University on December 21, 2014

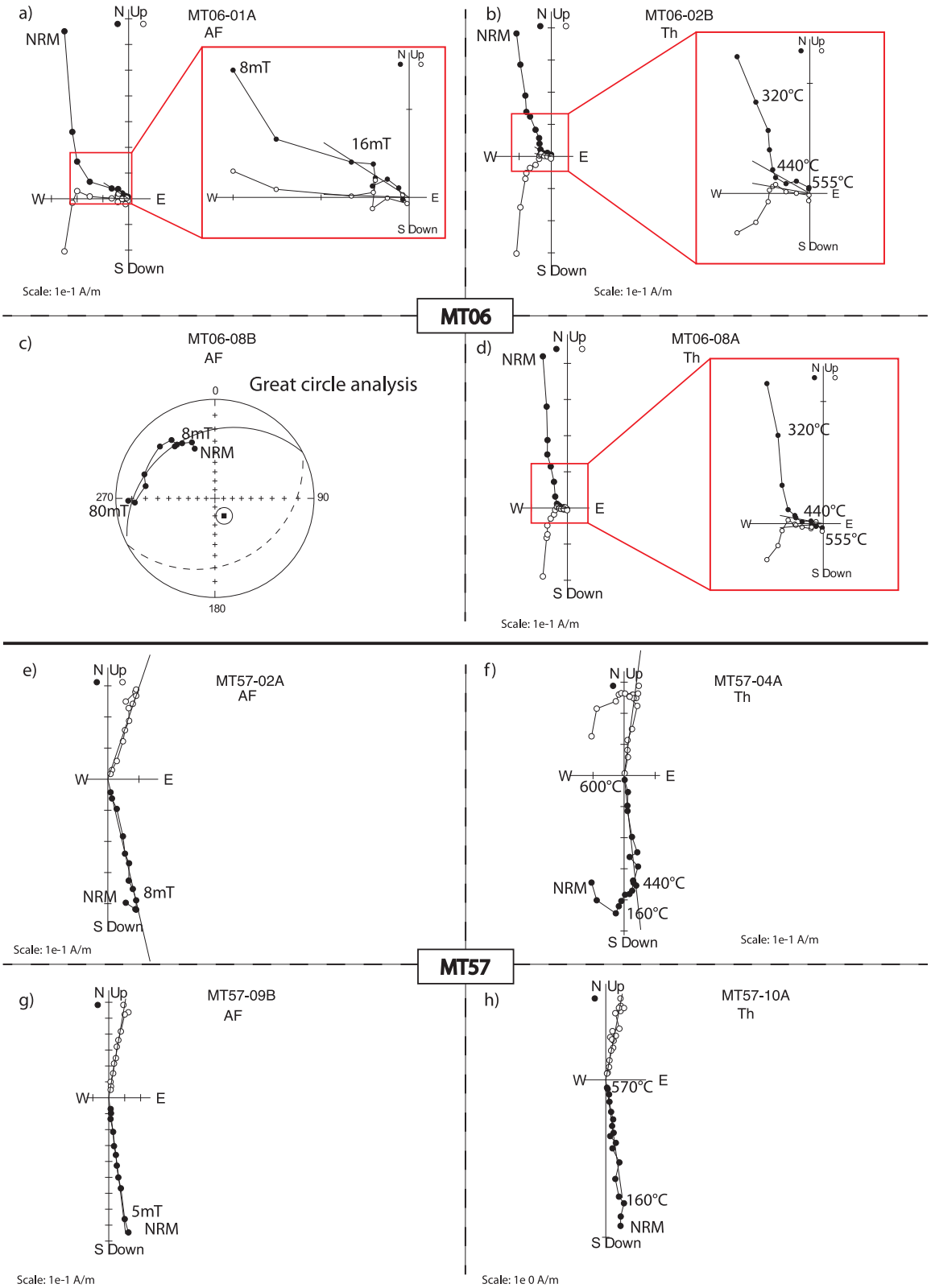

Figure 3. Demagnetization diagrams for site MT06 and MT57. Symbols are as in Fig. 2. Insets show zoom in demagnetization diagrams for site MT06.

a well-studied transitional flow from Steens Mountain was revisited using the Triaxe vibrating sample magnetometer (Coe *et al.* 2014). Monitoring of the directions during rapid continuous demagnetization demonstrated that a previously undetected VRM was mixed with the primary TRM and led to an erroneous interpretation when using conventional demagnetization techniques.

The Triaxe can also be used to track self-reversal mechanisms by carefully monitoring the temperature dependence of the

Downloaded from http://gji.oxfordjournals.org/ at Erciyes University on December 21, 2014

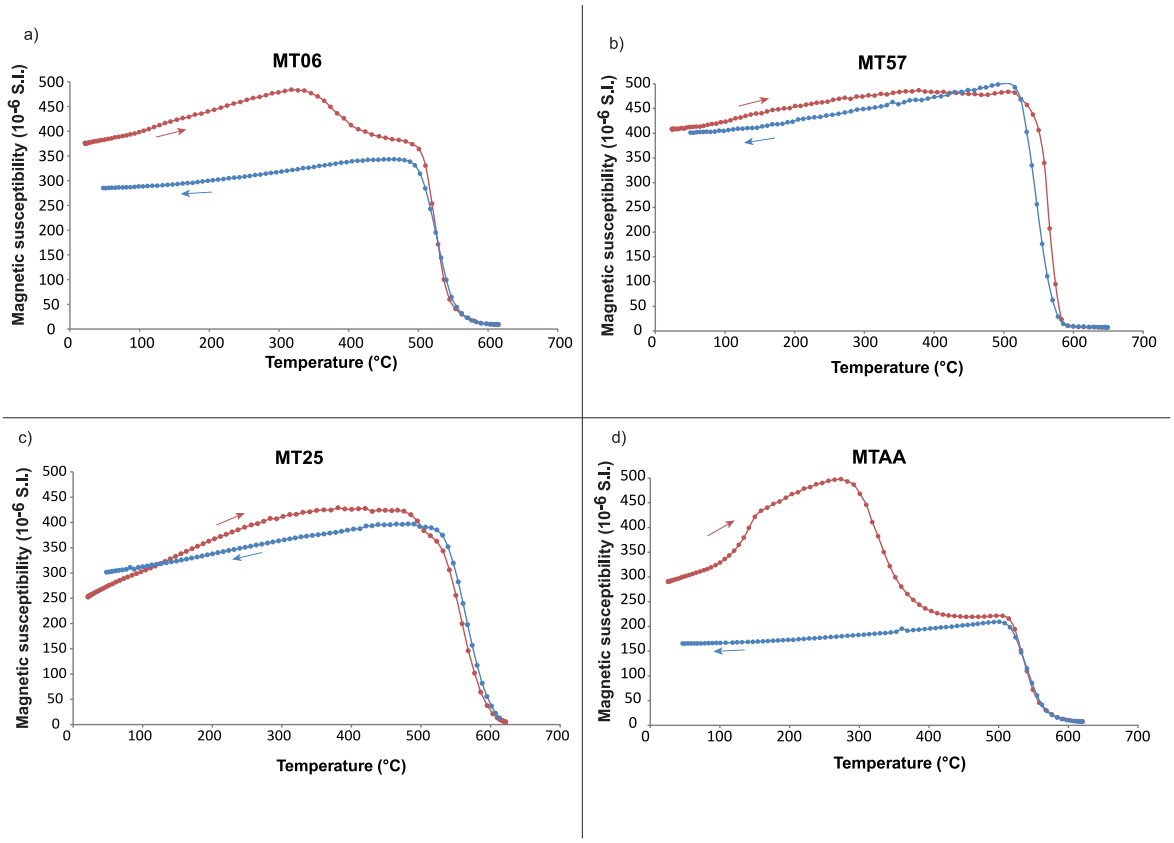

Figure 4. Thermomagnetic curves. Magnetic susceptibility versus temperature; (a) typical diagram of specimen showing the presence of Ti-low magnetite and maghemite and/or Ti-rich magnetite, (b, c) example of specimens characterized by a dominant phase of Ti-low magnetite with possibly a small fraction of Ti-hematite in (c), (d) specimen from site MTAA showing evidences for a transformation during heating. Heating, in red, and cooling, in blue, are also indicated by arrows.

spontaneous magnetization (Plenier *et al.* 2007). We monitored the magnetization of samples from sites MT06, MT16 and MT57 during several heating-cooling cycles as well as the evolution of the direction during continuous thermal demagnetization (Fig. 8). The magnetic moment of sample from site MT06 quickly reached the sensitivity limit of the Triaxe (∼2 × 10–8 Am^2) and therefore we restrained the maximum temperature of the cycles to 300 °C, a sister sample was still heated until 500 °C and its direction was monitored (Fig. 8a). Cycles were performed up to 520 °C for the other samples. No sample displayed a characteristic hump in the cooling curves which would reveal a partial self-reversal (Plenier *et al.* 2007) and the demagnetization curves neither showed any increase in magnetization which was interpreted as a hallmark of self-reversal by Heller & Petersen (1982). It is also significant that during these experiments the directions of the three samples evolved towards the corresponding site mean characteristic direction that was derived from stepwise thermal demagnetization. These results confirm the primary origin of the characteristic directions obtained at sites MT06, MT16 and MT57.

4.5 Hysteresis properties and IRM acquisition

All hysteresis curves are presented in Fig. S1 and a selection of four curves is shown in Fig. 9. All curves share strong similarities with the exception of site MTAC for which saturation was hardly reached due to the contribution of hematite (Fig. 9j). The mixture of magnetic grains with different compositions (cation deficient magnetite and titanium bearing magnetite) biases the analysis of magnetic grain sizes using the ratios J_{rs}/J_s versus H_{cr}/H_c (Dunlop 2002). However a rough estimate can be attempted given that (with the exception of MTAC) magnetite or Ti-poor magnetite dominates the magnetization in all samples. All samples follow the theoretical mixing curves with J_{rs}/J_s values from 0.05 to 0.2 and H_{cr}/H_c ratios from 2 to 5.6, so that magnetic carriers are leaning towards a SD/MD mixture with a significant MD component (Dunlop 2002).

The IRM acquisition curves (Figs 9b, e, h and k) show that the main magnetic carrier is a low coercive phase reaching saturation above 100 or 150 mT except at site MTAC. Unmixing of raw IRM curves by CLG functions (Kruiver *et al.* 2001) isolates one to three magnetic components contributing to the high field remanence (Figs 9c, f, i, l and Fig. S2 and Table S1). The components 1 and 2 correspond to low coercive phases. The mean acquisition field (B1/2) of the dominant phase (component 2) is comprised between 30 and 65 mT while component 1 has a softer coercivity with B1/2 between 15 and 25 mT (Table S1). Both likely correspond to a mixture of Ti-magnetite with varying grain sizes, Ti-content and/or cation deficiency (Kruiver *et al.* 2001). The hard fraction component observed in samples from sites MT06, MT38, MTAC and MT101 has a mean acquisition field varying between 300 and 800 mT and thus typical of hematite. This component has a small contribution except for site MTAC (Fig. 9l). At this point, it is interesting to note that the presence of hematite was deduced from the thermomagnetic experiments conducted at sites MT38, MT101 and MTAC as well as for MT08, MT16 and MT25. No hematite has been detected at site MT06. This may reflects some mineralogical variability within

Downloaded from http://gji.oxfordjournals.org/ at Erciyes University on December 21, 2014

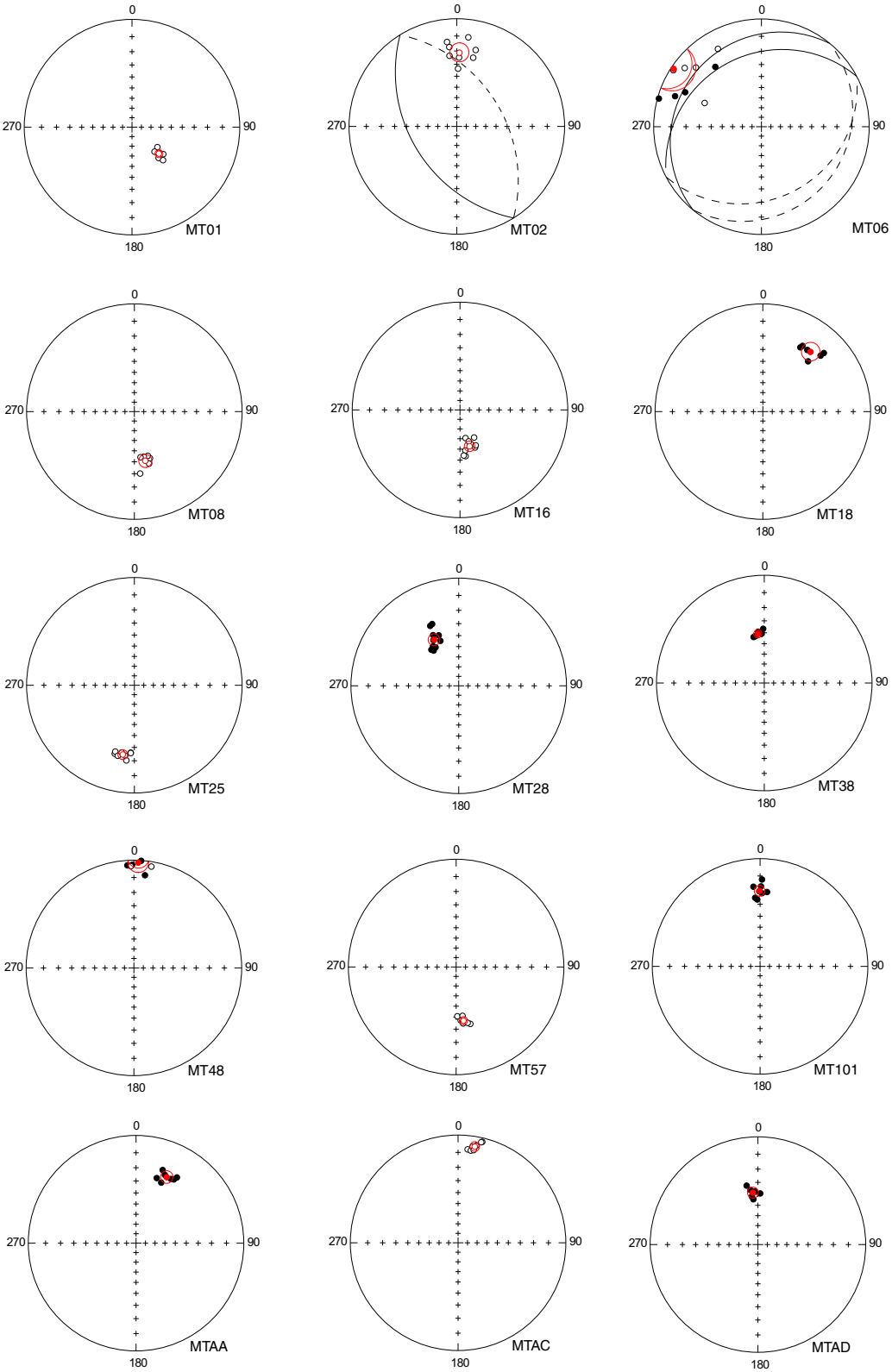

Figure 5. Stereoplots for each sites.

these sites, but we can neither exclude the nucleation of a tiny high coercivity phase during laboratory thermal treatment. In all cases, the signal remained very weak, and sometimes hardly resolvable with the notable exception of site MTAC.

4.6 SEM observations

SEM observations of polished thin sections of sites MTAA, MTAC, MT06, MT38, MT57 and MT101 always revealed case a mixture of large iron oxide grains, euhedral to dendritic, with size varying from

Downloaded from http://gji.oxfordjournals.org/ at Erciyes University on December 21, 2014

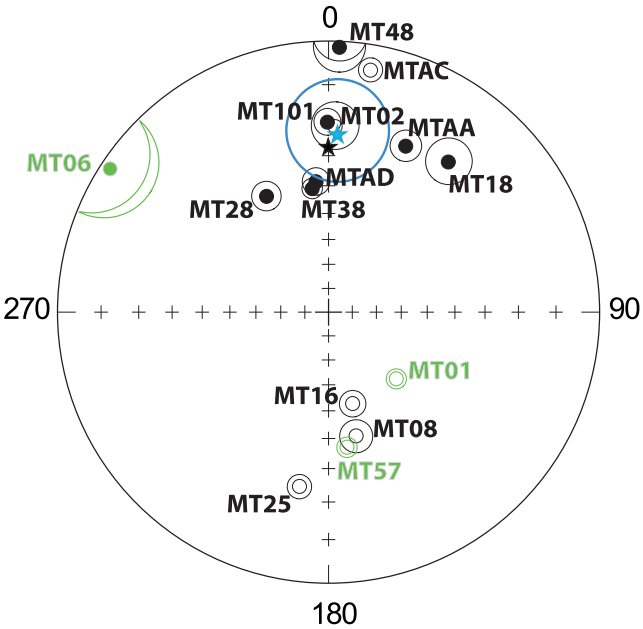

Figure 6. Palaeomagnetic directions. Equal area projection of the mean palaeomagnetic directions obtained for each flow with their associate 95 per cent confidence cones. Closed and open symbols indicate positive and negative inclination, respectively. The mean direction derived from all sites (except site 06) is plotted as a blue star with confidence interval shown at 95 per cent. Black star indicates dipole field at Martinique Island. Sites in green are associated to anomalous directions.

10 to 100 μm. This population is mixed with smaller grains of 1–5 μm diameter lying in a silicate matrix. Representative photographs for sites MT06, MT57 and MTAC are presented in Fig. 10. Most grains, even the small ones, show oxy-exsolution features forming alternating lamellae of different compositions (Figs 10a–c). EDS-X analyses indicate that the titanium and iron compositions of exsolved latches are probably linked to ilmenite. Cracks sometimes occur, especially along the larger grains (Fig. 10b) probably caused by shrinking of the primary Ti-magnetite lattice during oxidation to cation-deficient Ti-maghemite. In sample MTAC small hematite grains (1 μms or less) are clustered into large red coloured areas up to 1 mm in size (Figs 10e and f), while larger magnetite grains lie around the clusters (Fig. 10e).

5 DISCUSSION

5.1 Magnetostratigraphic aspects

The palaeomagnetic directions from Table 1 have been plotted as a function of time in Fig. 11 along with the most recent geomagnetic polarity timescale (Gee & Kent 2007). Four sites with reverse polarity (MT01, MT08, MT16 and MT25) are consistently found between 1.6 and 2.3 Ma and belong to the reverse polarity Matuyama interval. An interesting observation is that site MT01 with a low VGP latitude (−45.3°) and an age of 1.69 ± 0.02 Ma is positioned within the geomagnetic instabilities associated with the Gilsa subchron (∼1.6 Ma old, Udagawa *et al.* 1999). Two others were erupted during the Olduvai Normal polarity subchron (MT101 and MT38) and show the expected normal polarity directions. The 9 remaining sites with ages between 770 and 9 ka belong to the Brunhes Normal polarity chron. Seven sites have a full normal polarity. We discuss below the origin of the large deviations found for the other two sites (MT06 and MT57).

5.2 Origin of the «anomaleous» directions

Site MT06 is characterized by a low VGP latitude at 32.7° and an age at 770 ± 11 ka (Samper *et al.* 2008) which corresponds exactly to the age derived from recent compilations of the most detailed records of the last reversal (Singer *et al.* 2002; Channell *et al.* 2010; Valet *et al.* 2014). The existence of a tiny persistent secondary component combined with a rather large dispersion (low *k*) is also a distinctive feature of this site. Such behaviour is not rare in transitional

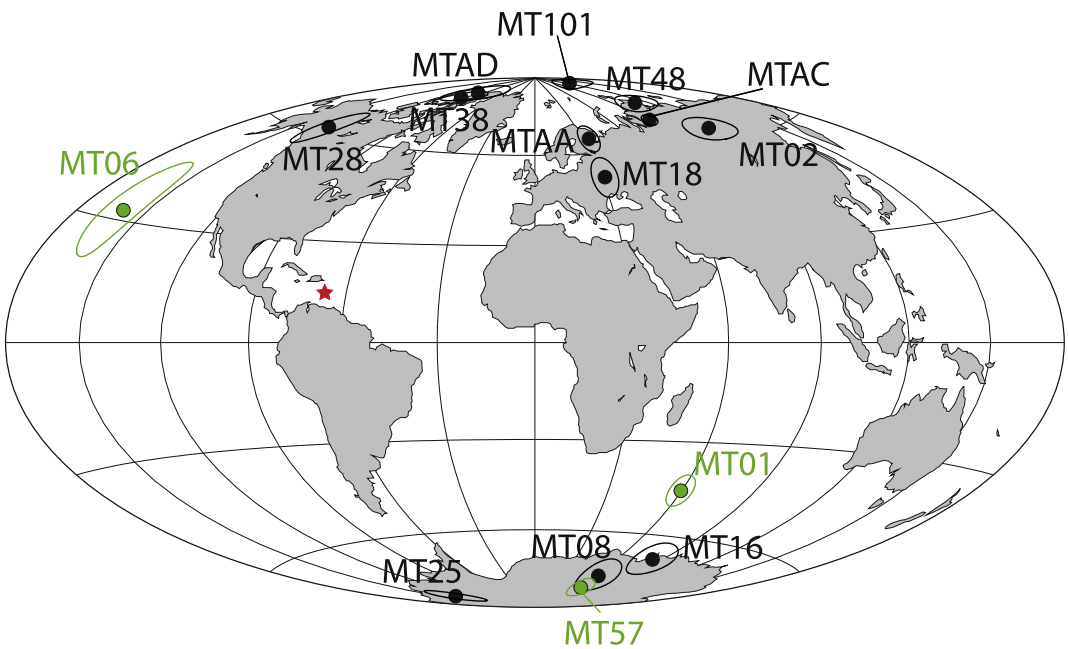

Figure 7. Virtual Geomagnetic poles (VGPs). Earth projection of the geographic positions of the VGPs with their 95 per cent confidence cones. Site locations (Martinique Island) are plotted as a red star. VGPs in green are associated to anomalous directions.

Downloaded from http://gji.oxfordjournals.org/ at Erciyes University on December 21, 2014

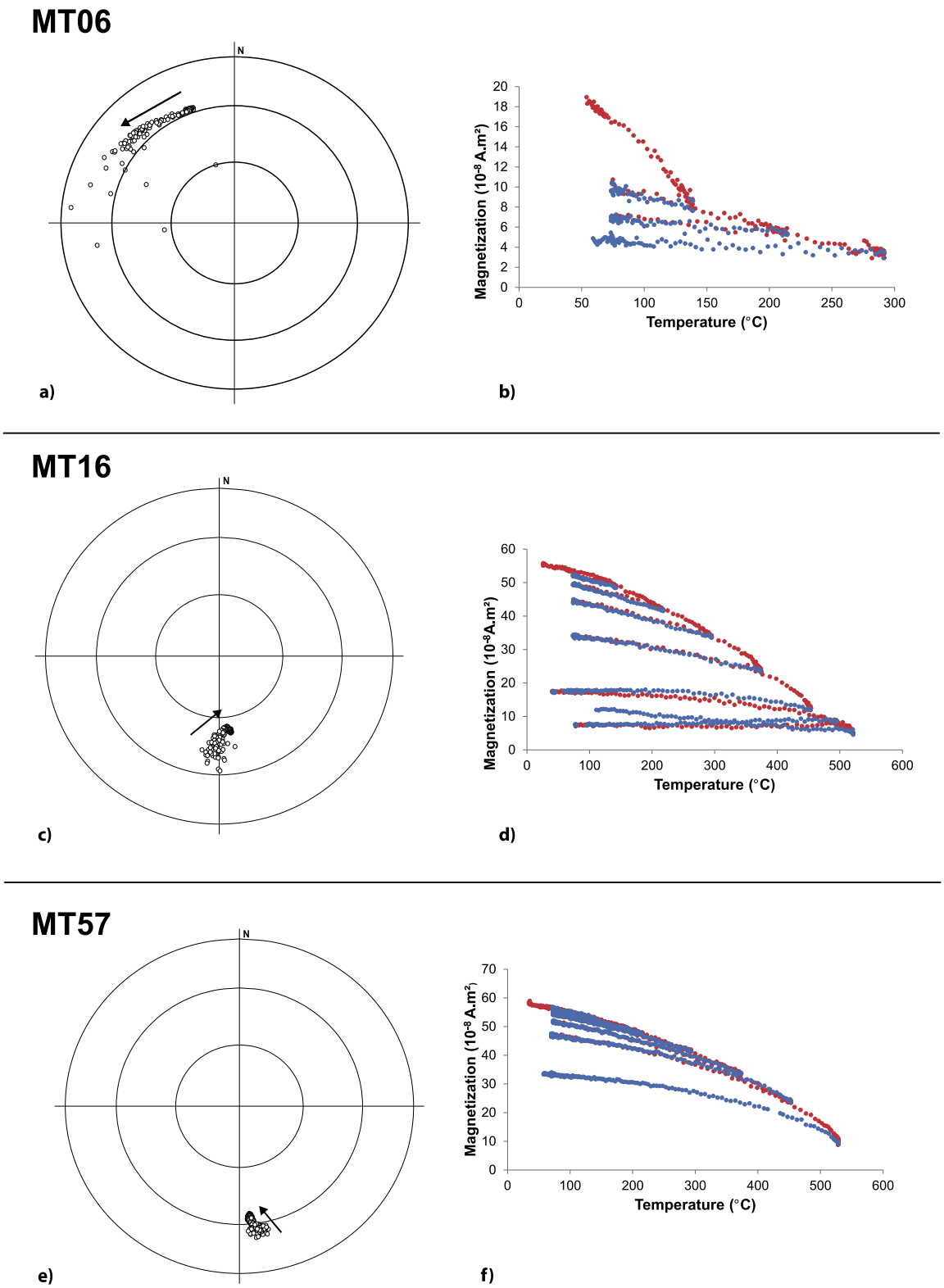

Figure 8. Triaxe experiments. Directions in equal area projection (left-hand side) and intensity of the magnetization (right-hand side) during continuous thermal demagnetization cycles in the Triaxe vibrating sample magnetometer of samples from site MT06 (a, b), MT16 (c, d) and MT57 (e, f). Arrows indicate low to high temperature, red is heating and blue cooling.

lava flows (see e.g. Quidelleur & Valet 1996). Given the very low field intensity prevailing during reversals, it is possible that rapidly time-varying multipolar components can be recorded during cooling of a transitional flow. We cannot neglect also that the external field is expected to be more active so that magnetic storms generate additional spurious components. Finally, the relative imprint of tiny hard viscous components which are usually not even detected would also contribute to increase the dispersion in presence of a very weak

Downloaded from http://gji.oxfordjournals.org/ at Erciyes University on December 21, 2014

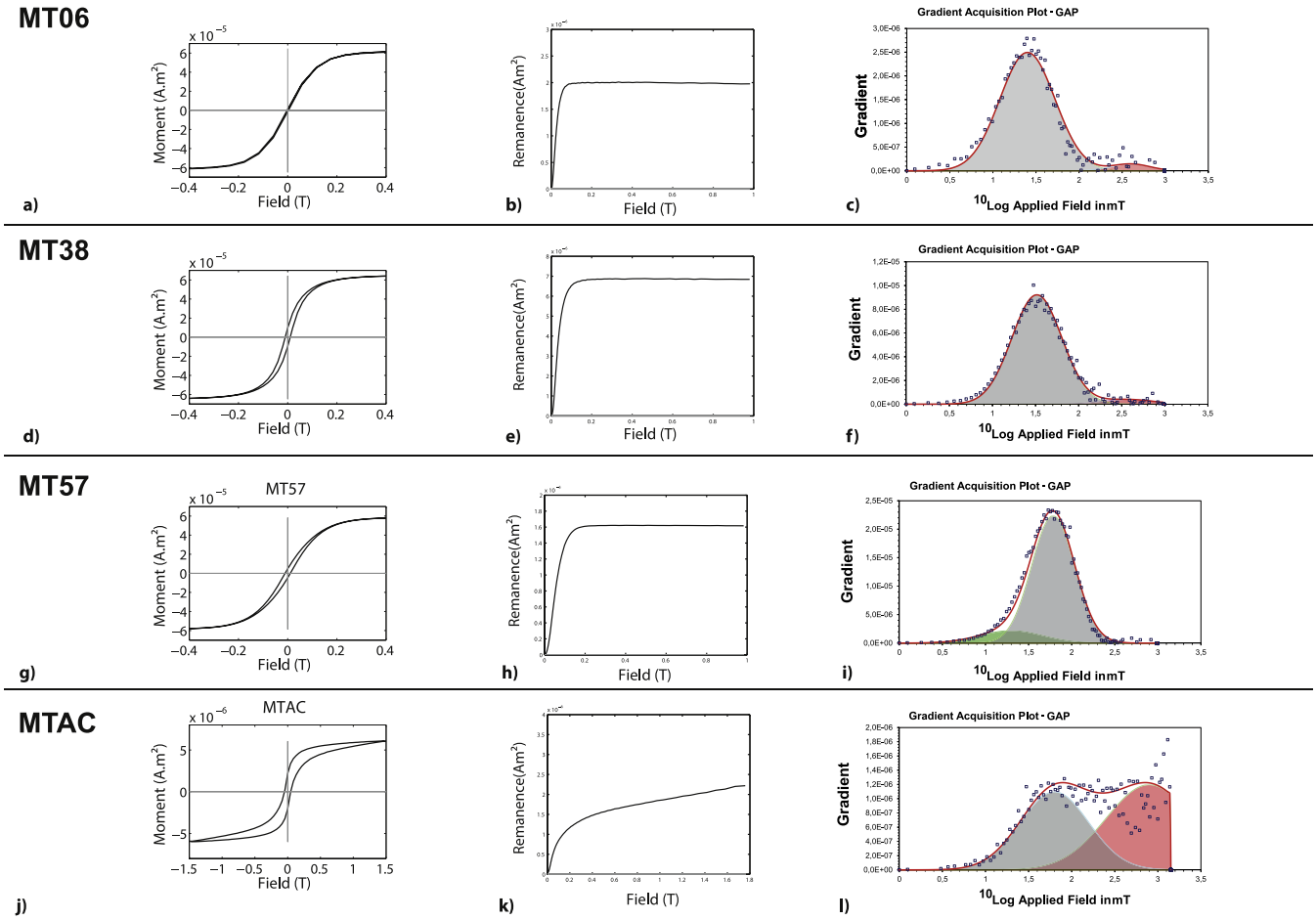

Figure 9. High-field properties. Hysteresis curves (left-hand side), raw isothermal remanent magnetization curves (middle) and treatment of the IRM data by the cumulative log-Gaussian (CLG) function (Kruiver *et al.* 2001) (right-hand side) for samples from site MT06, MT38, MT57 and MTAC. CLG analyses show that all samples are dominated by unimodal to bimodal distribution, attributed to a mixed populations of Ti-magnetite (in green and grey) and sometimes a contribution of hematite (in red) especially for site MTAC.

characteristic TRM. We thus interpret the secondary component, relatively high dispersion and anomalous directions of MT06 as the hallmark of a low and transitional magnetic field which prevailed during the Matuyama–Brunhes transition. Interestingly, the last reversal has also been recorded by a 777 ± 14-ka-old lava unit from the nearby island of Guadeloupe (Carlut *et al.* 2000). The palaeomagnetic analysis (GU09 site) indicated also a transitional direction with a VGP located at 27.4°S and 217.8°E. This location is 60° south to the VGP from MT06 site (32.7°N; 200°E) in Martinique, but is more or less located along the same longitude in the middle Pacific. These two sites from the Caribbean region should help constrain the field geometry during the last geomagnetic reversal.

Site MT57 has a fully reversed palaeodirection but an age of 617 ± 52 ka which cannot be reconciled with the last reversal. The age uncertainty for this site is unfortunately rather large and is explained by a large amount of atmospheric argon contamination in the samples. Considering the young age of this lava dome and its relatively low potassium content (Germa *et al.* 2011) it is difficult to envision reducing the age uncertainty although future resampling is considered by the authors. Geomagnetic excursions have been reported within this age window, but confusion about their exact number is generated by dating uncertainties and also by the complexity of the field geometry during these events. A global compilation of the Brunhes geomagnetic instabilities (Lund *et al.* 2006) that have been reported from sedimentary records summarizes a total of 17 excursions with their ages derived from carbonate and oxygen isotope stratigraphy. Three events, BigLost/CR3 (∼575 ka), La Palma/15β (∼605 ka) and Delta/17α (∼665 ka) fall within the age window of site 06MT57 and are thus potential candidates.

The Big Lost/CR3 excursion was first found in Idaho from a group of four reversely magnetized flows (Champion *et al.* 1981; Champion *et al.* 1988). The K–Ar weighted mean age for these flows is 565 ± 14 ka (Champion *et al.* 1988) and there is a slightly younger $^{40}Ar/^{39}Ar$ age at 558 ± 20 ka for one of the reversed flows (Lanphere 2000). More recently, several transitional units from Tahiti-Nui (Hoffman & Singer 2004) with $^{40}Ar/^{39}Ar$ ages at 579 ± 9 ka were interpreted as markers of the Big Lost event. Thus, taking into account the discrepancies between the different dates, an unweighted radiometric mean age emerges at ∼567 ± 14 ka and places the Big Lost event within the lower age range derived from the K–Ar dating of site MT57 at Martinique Island.

The La Palma/15β event was initially described from a succession of 12 lava units from the La Palma Island (Quidelleur & Valet 1996) that have recorded transitional directions. K/Ar dating assigned an age of 602 ± 12 ka to this event (Quidelleur *et al.* 1999). In a subsequent study of the same flows, Singer *et al.* (2002) reported a mean weighted $^{40}Ar/^{39}Ar$ age of 580 ± 8 ka and suggested that the La Palma event would actually be correlated with the Big

Downloaded from http://gji.oxfordjournals.org/ at Erciyes University on December 21, 2014

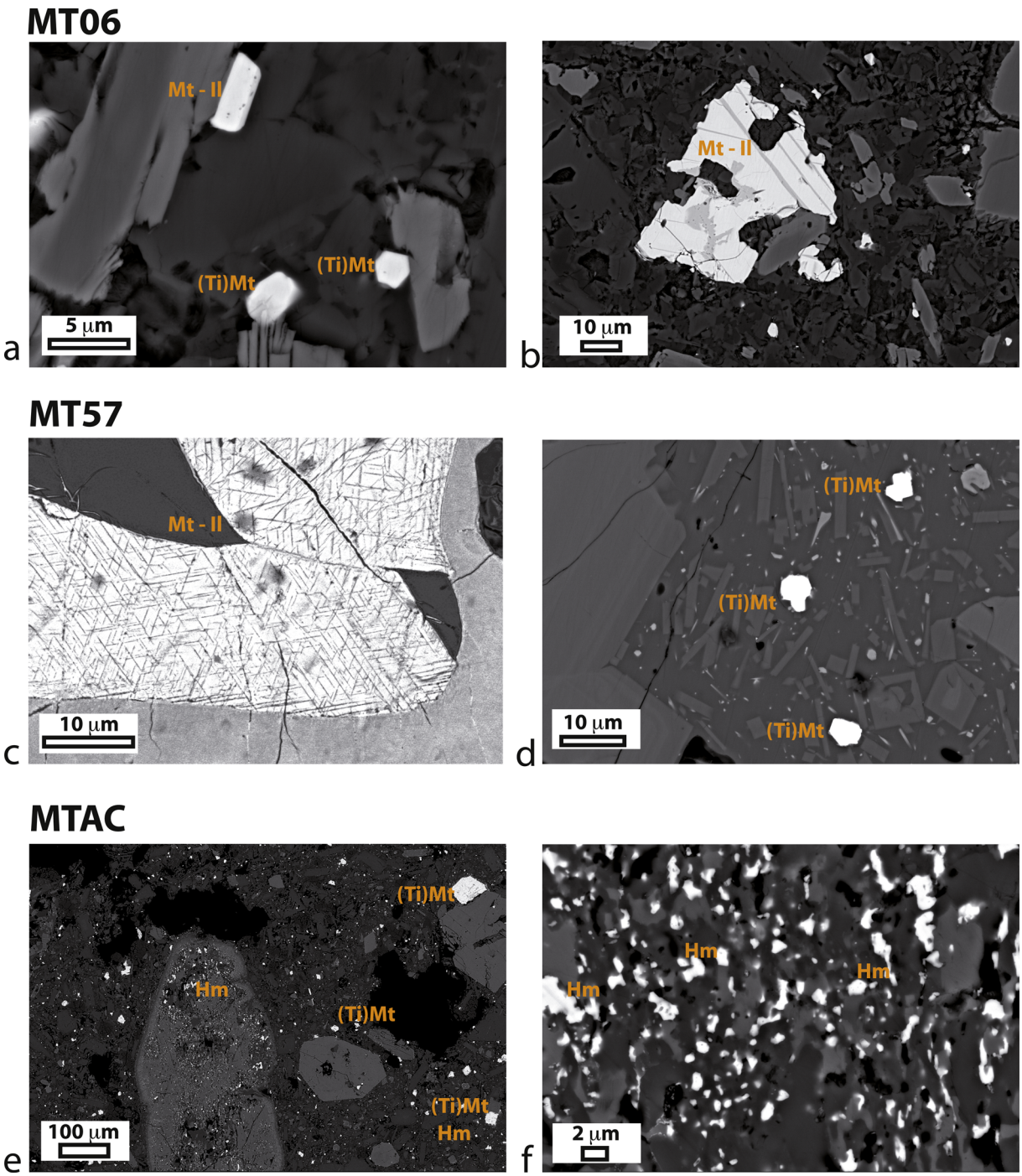

Figure 10. SEM Photographs. Representative SEM photos of iron oxides for sites MT06 (a, b), MT57 (c, d) and MTAC (e, f). Most grains, even the small ones, show oxy-exsolution features forming alternating lamellae of Ti-poor-magnetite and ilmenite (a, b, c). Cracks can sometimes be observed (b, c) suggesting some degree of maghemitization. (f) is a zoom of (e) corresponding to the white rectangle and shows cluster of small hematite grains.

Lost excursion. The origin of the discrepancy between these two sets of ages has not been fully resolved yet. However, two reversed polarity flows from Western Mexico have been recently dated by $^{40}Ar/^{39}Ar$ (Petronille *et al.* 2005). Their ages at 614 ± 16 and 623 ± 91 ka combined with the K/Ar ages from La Palma pleads in favour of an excursion with fully reversed directions at ∼613 ± 39 ka (unweighted radiometric ages). We speculate that the concordance in the ages of these lava flows with transitional to fully reversed directions at the three localities (La Palma, Western Mexico and La Martinique) is not fortuitous. It should be noted that this period is also coeval with four transitional flows with a mean radiometric $^{40}Ar/^{39}Ar$ age at 626 ± 24 ka from the West Eiffel province (Germany) (Schnepp 1996; Singer *et al.* 2008).

Finally, the Delta/17α event was mostly reported from sedimentary records (Creer *et al.* 1980; Biswas *et al.* 1999; Carcaillet *et al.* 2004; Lund *et al.* 2006) with ages from 665 to 700 ka. The unique volcanic record of this event was recently found in Western Mexico with a radiometric $^{40}Ar/^{39}Ar$ dating at 671 ± 13 ka (Lewis-Kenedi *et al.* 2005; Ceja *et al.* 2006). This age would position the Delta event at an upper limit for MT57.

Downloaded from http://gji.oxfordjournals.org/ at Erciyes University on December 21, 2014

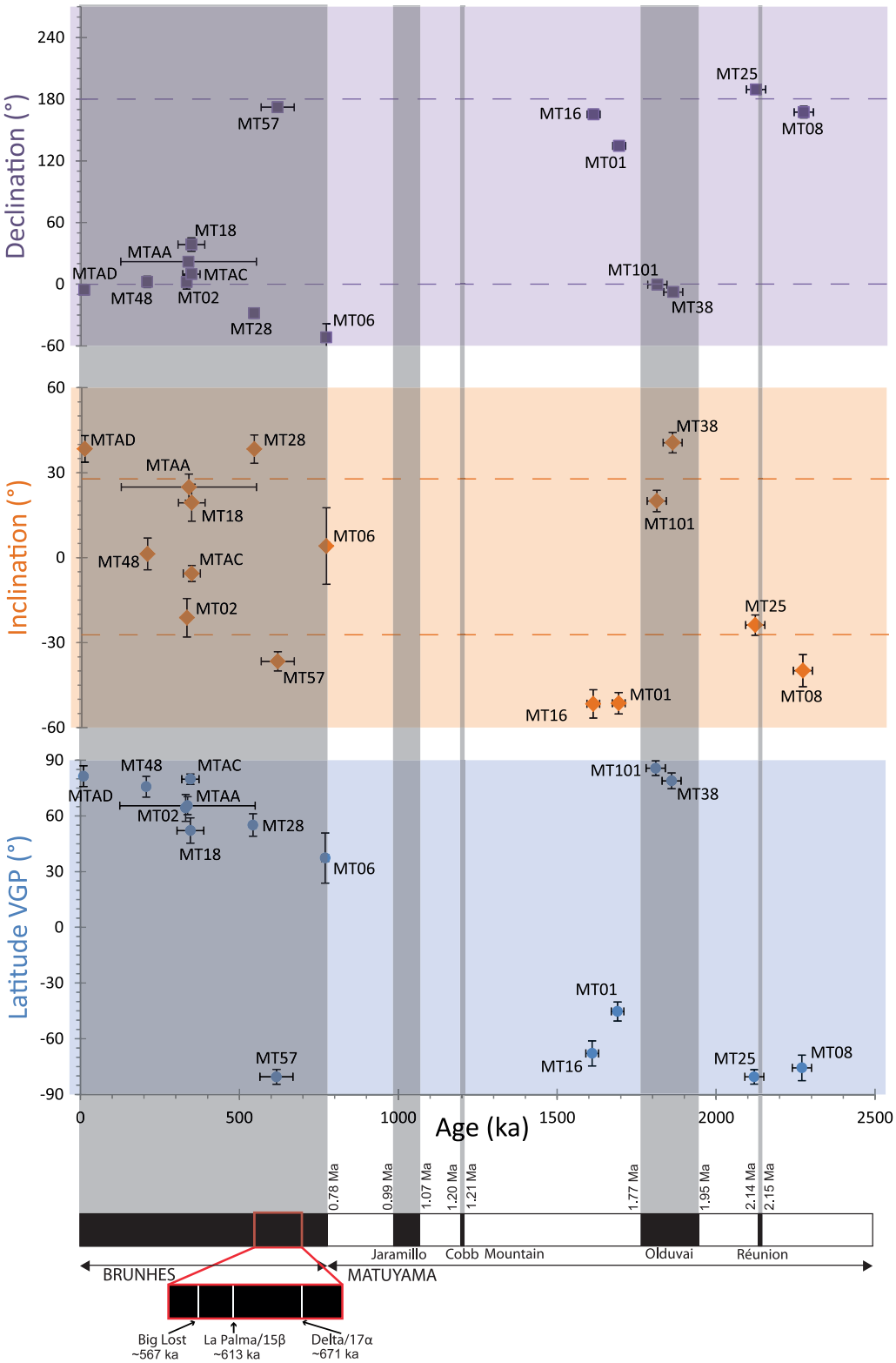

Figure 11. Directional changes. Evolution of palaeomagnetic declination, inclination and VGP latitude as a function of time for the 15 sites. The direction expected for the axial dipole field at Martinique Island is shown by dashed lines. A geomagnetic polarity timescale (Cande & Kent 1995; Lund *et al.* 2006), is shown at bottom [black (resp. white) represent normal (resp. reverse) polarity].

This summary of the Brunhes instabilities within the age window of site MT57 tells us that the La Palma/15b event is the best candidate. To our knowledge, four volcanic records of excursions, Laschamp (~40 ka), Blake (~115 ka), Pringle falls (~220 ka) and Big Lost (~567 ka) exhibit fully reverse directions within the Brunhes (see Bonhommet & Babkine 1967; Champion *et al.* 1988; Zanella 1998; Calvo-Rathert *et al.* 2013). The present results from site MT57 and a former study by Petronille *et al.* (2005) argue for

Downloaded from http://gji.oxfordjournals.org/ at Erciyes University on December 21, 2014

Table 2. Mean magnetic field. Column headings indicate: Mean directions, inclination and radius of the 95 per cent confidence cone and the VGP scatter with its upper and lower limits for various selections of the data set.

		Mean direction			Palaeopole				
N	Excluded site	D_m	I_m	α_{95}	Long.	Lat.	Sb	lSb	uSb
14	MT06	359.7	27.1	14.2	234.9	88.2	23.3	18.6	31.2
13	MT06 and MT01	2.1	24.7	13.9	66.1	88.6	20.5	16.3	27.8
13	MT06 and MT57	0.3	26.3	15.4	226.2	88.8	24.1	19.1	32.6
12	MT06, MT01 and MT57	2.9	23.6	15.0	66.9	87.6	21.3	16.8	29.2

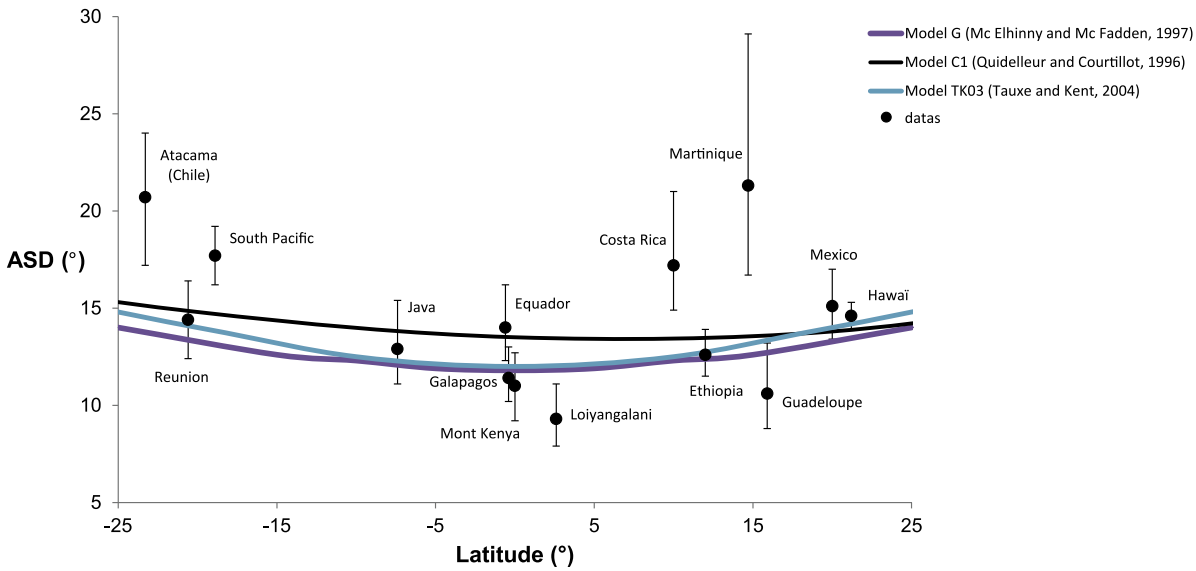

Figure 12. Dispersion of poles. VGP scatter (Sb) as a function of site latitude with 95 per cent confidence intervals (errors bars) for this study and a global database. Model G from (McElhinny & McFadden 1997), model C from (Quidelleur & Courtillot 1996) and model TK03 from (Tauxe & Kent 2004) are plotted in violet, black and blue, respectively.

the existence of another reversed event at least in the Caribbean and central Americas at ~613 ka which would thus be the fifth Brunhes reversed event from volcanic rocks. Multiple records from different locations are evidently mandatory to assess the field geometry during these episodes but the fact that five geomagnetic intervals within the Brunhes exhibit reversed direction is appealing and suggests a few remarks regarding the field structure during these events.

Simple models simulating a reduction of the dipole to 10 per cent of its original value (Valet *et al.* 2012) and therefore the dominance of the non-dipolar components, show that the presence of full reversed directions at distinct locations is almost impossible. We infer that these reversed directions cannot be explained by an episode of large amplitude secular variation (Valet *et al.* 2008), and indeed were produced by a reversed dipole that dominated during a short time period. The finding of reversed directions at different localities also suggests that such events are significant and long enough for leaving us a chance to detect the record in distinct volcanic series.

5.3 Time averaged field, VGP scatter and inclination anomaly

The mean directions derived from various subsets of data (excluding site MT06 only or a combination of sites MT06, MT57 and/or MT01) are characterized by declinations between −0.3° and 2.9° and inclinations between 23.6° and 27.1° (the expected dipole inclination is 27.5°) with a α_{95} around 15°. These results are fully compatible with the geocentric axial dipole hypothesis. Selecting only normal polarity sites within the Brunhes yields Dec = 7.4°, Inc = 14.1°, $k = 7.5$ with $\alpha_{95} = 23.6°$, which is also compatible with the axial dipole hypothesis. Unfortunately, the small number of reversely magnetized flows does not allow to derive meaningful statistical characteristic.

The latitudinal variation in dispersion of the virtual geomagnetic poles is another informative characteristic of the TAF (Cox 1962, 1969; McElhinny & Merrill 1975; McElhinny & McFadden 1997). The measured dispersion of VGPs is a combination of the scatter caused by secular variation but also the within-site scatter due to uncertainties in the measurements and sampling. The angular deviation of VGPs, which represents the angular dispersion with respect to the rotation axis, was thus calculated by substracting the within-site scatter using the formula:

$$Sb = \sqrt{\frac{1}{N-1}\sum_{i=1}^{N}\left[\Delta_i^2 - \left(\frac{N-1}{N}\right)\left(\frac{S_{wi}^2}{N_{si}}\right)\right]},$$

where N is the number of sites, Δ_i represents the angular deviation of the pole for the ith site from the geographic North Pole, and S_{wi} is the within-site dispersion determined from N_{si} samples at each site.

Estimates of Sb with its upper and lower limits (lSb and uSb) are reported in Table 2 for various subdata sets. For the Martinique set, excluding MT06, MT57 and MT01, the dispersion is 21.3°, while a mean value of 13–14° is predicted (Fig. 12, Table 3) by Model C, G or TK03 (Quidelleur & Courtillot 1996; McElhinny &

Downloaded from http://gji.oxfordjournals.org/ at Erciyes University on December 21, 2014

Table 3. VGP scatter. Mean scatter of VGP for this study and a global data set between −25° and +25° of latitude. Column headings indicate: site name, site latitude, site longitude, number of data used, between-site dispersion of VGP, lower and upper bounds of 95 per cent confidence interval using method of Cox (1969), reference.

Localization	sLat (°)	sLon (°)	*N*	ASD (°)	Sl (°)	Su (°)	Reference
Atacama. Nothern Chile	− 23.3	292.3	36	20.7	17.2	24	Johnson *et al.* (2008)
Compilation Reunion	− 20.6	56.5	84	14.4	12.4	16.4	Compilation from Lawrence *et al.* (2006)
Compilation South Pacific	− 18.9	189.1	280	17.7	16.2	19.2	Compilation from Lawrence *et al.* (2006)
Java	− 7.4	112	35	12.9	11.1	15.4	Elmaleh *et al.* (2004)
Equador	− 0.6	282	51	14	12.3	16.2	Opdyke *et al.* (2006)
Galapagos	− 0.4	268.4	64	11.4	10.2	13	Kent *et al.* (2010)
Mt Kenya	0	36.5	69	11	9.2	12.7	Opdyke *et al.* (2010)
Loiyangalani	2.6	36.5	32	9.3	7.9	11.1	Constable & Parker (1988)
Costa Rica	10	276	28	17.2	14.9	21	Johnson *et al.* (2008)
Ethiopia	12	41.5	103	12.6	11.5	13.9	Kidane *et al.* (2003)
Martinique	14.7	298.9	12	21.3	16.7	29.1	This study
Guadeloupe	15.9	298.2	23	10.6	8.8	13.2	Carlut *et al.* (2000)
Compilation Mexico	20	258.6	216	15.1	13.4	17	Conte-Fasano *et al.* (2006); Goguitchaichvili *et al.* (2007); Compilation from Lawrence *et al.* (2006); Peña *et al.* (2009); Sbarbori *et al.* (2009); Calvo-Rathert *et al.* (2013); Peña *et al.* (2014)
Compilation Hawaï	21.2	200.2	766	14.6	13.9	15.3	Compilation from Lawrence *et al.* (2006)

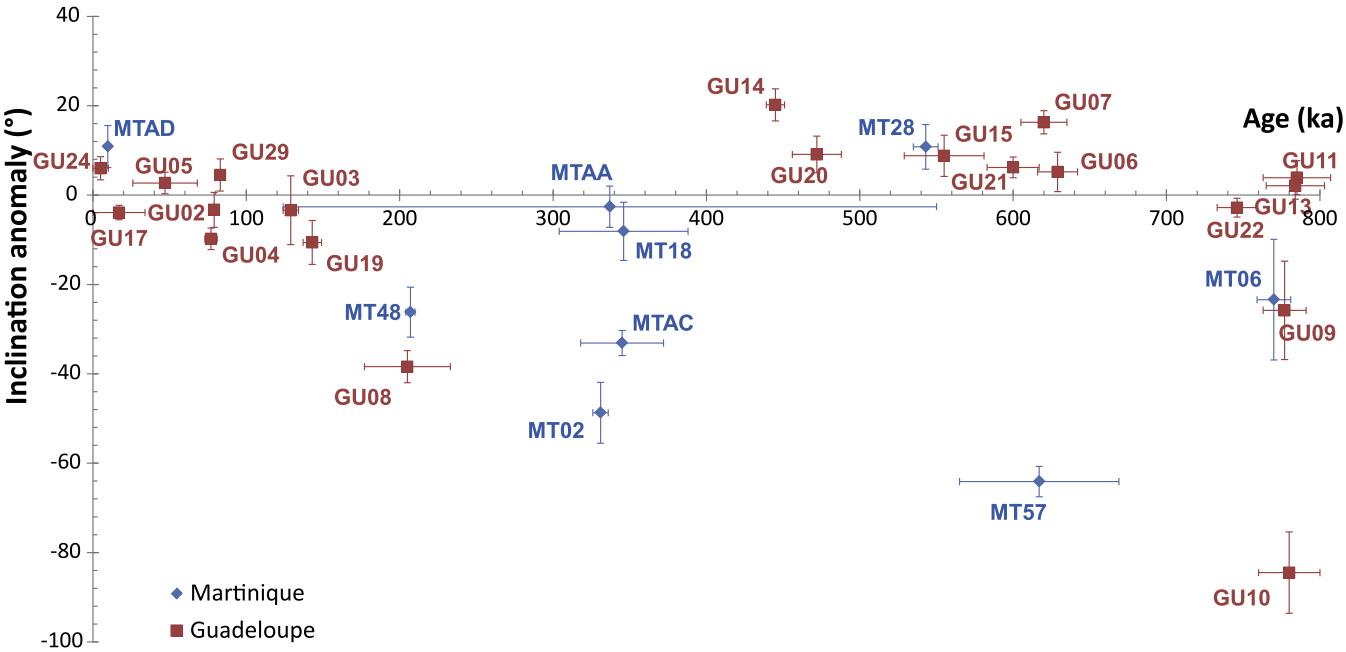

Figure 13. Inclination anomaly. Deviation between each mean-site direction and the inclination of the axial dipole versus age for Guadeloupe Island (Carlut *et al.* 2000) and Martinique Island (this study) dated flows between 0 and 800 ka.

McFadden 1997; Tauxe & Kent 2004) at these latitudes. Such large dispersion may be related to the small size of the data set which includes 12 sites only after excluding all excursional or transitional directions. A particularity of our set is also that the high density of flows with ages around 350 ka which corresponds to a well-known episode of intense volcanism (Boudon *et al.* 2013). It is possible that period of large secular variation (revealed by flows MT18, MT02 and MTAA) has been oversampled within this age window. In any case, the relatively large dispersion in Martinique is fully consistent with results from other low latitude sites like Costa Rica in the northern hemisphere as well as with the South Pacific compilation and the Atacama data from the southern hemisphere.

Despite the absence of significant deviation of the time-averaged inclination from the axial dipole field, we can investigate whether some periods exhibit persisting features that could be indicative of a long-term anomaly. We restrained the data set to the Brunhes chron which incorporates the largest number of results. The evolution of inclination anomaly ($\Delta I = I_{\mathrm{mes}} - I_{\mathrm{GAD}}$) is plotted in Fig. 13 along with previous results from the nearby La Guadeloupe Island. To some degree the Martinique and Guadeloupe inclination data show mostly negative inclination anomalies for the 100–400 ka period and positive ones over the 400–700 ka period. However this observation which has previously been reported (Carlut *et al.* 2000) should be regarded with caution. Because of the large dispersion around 350 ka in the Martinique Island data set (with important anomalies at sites MT02 and MTAC), it may also result from some peculiar geometry of the field at that time. Other studies of palaeosecular variation have suggested the existence of anomalies over periods of a few tens of ka during the Brunhes (Elmaleh *et al.* 2004). Unfortunately, the database is still too small to infer statistically robust features,

Downloaded from http://gji.oxfordjournals.org/ at Erciyes University on December 21, 2014

and emphasizes the interest of collecting new data from different time intervals to constrain the geomagnetic field models.

6 CONCLUSION

This study conducted from 23 lava flows from the Martinique island provided 15 suitable mean site directions. Three sites exhibit excursional directions with VGP latitudes more than 40° away from the local axial dipole direction. This corresponds to 20 per cent of the total directions and is in excellent agreement with the 17.5 per cent of VGPs lower than 50° derived from the global database. Another interesting characteristic is the large dispersion of the directions (after removing the sites with intermediate polarity) which results in a VGP scatter ∼5° higher than the values predicted by the current models at this latitude. In addition to field observations and tectonic studies performed ahead of the present work, no evidence for local blocks displacements can be put forward as a possible cause of dispersion. Whether this larger scatter reflects a bias imposed by non-dipolar standing field components constrained by the non-dipole/dipole field ratio in the island during the periods under investigation is plausible, but remains to be tested further. A few marine cores taken in the immediate vicinity of the island (Le Friant *et al.* 2013) will hopefully help clarify this question. The geomagnetic origin of the transitional directions is also not questioned and their age fits with other remarkable events that have been reported from other locations. The most obvious one is the Matuyama–Brunhes reversal with an age of 770 ± 11 ka obtained at La Martinique which is fully consistent with the 777 ± 14 ka found at the nearby island of La Guadeloupe and with most dates derived from orbitally tuned sedimentary records as well as from radiometric ages from volcanics. Another finding is the additional evidence for the existence of La Palma event (∼613 ka) initially discovered in the Canary islands, and more recently measured in lavas from western Mexico. The presence of reversed directions associated with this event reinforces the concept of an aborted field reversal as it is impossible to produce reversed directions over such a large area without a dominant reversed dipole (Valet *et al.* 2014).

ACKNOWLEDGEMENTS

We thank the editor and two anonymous reviewers for their critical suggestions which helped improve the paper. We thank Georges Boudon and Xavier Quidelleur for helpful discussions and indications for sampling. We are very grateful to the people from the Martinique volcanological observatory and specifically to Valérie Clouard for permanent help and lodging assistance. Damien Deldique and Maxime le Goff contributions to the experiments were greatly appreciated. This study was supported by the French INSU-CNRS program and IPGP UMR7154. This is IPGP contribution number 3579.

REFERENCES

Aubaud, C., Athanase, J.-E., Clouard, V., Barras, A.-V. & Sedan, O., 2013. A review of historical lahars, floods, and landslides in the Prêcheur river catchment (Montagne Pelée volcano, Martinique island, Lesser Antilles), *Bulletin de la Societe Geologique de France,* **184,** 137–154.

Biswas, D., Hyodo, M., Taniguchi, Y., Kaneko, M., Katoh, S., Sato, H., Kinugasa, Y. & Mizuno, K., 1999. Magnetostratigraphy of Plio-Pleistocene sediments in a 1700-m core from Osaka Bay, southwestern Japan and short geomagnetic events in the middle Matuyama and early Brunhes chrons, *Palaeogeog. Palaeclimat. Palaeoecol.,* **148,** 233–248.

Bonhommet, N. & Babkine, J., 1967. Sur la presence d'aimantations inversées dans Ia Chaine des Puys, *C.R. Acad. Sci. (Paris), Ser. B,* **264,** 92–94.

Boudon, G., Le Friant, A., Komorowski, J.C., Deplus, C. & Semet, M.P., 2007. Volcano flank instability in the Lesser Antilles Arc: diversity of scale, processes, and temporal recurrence, *J. geophys. Res.: Solid Earth (1978–2012),* **112,** B08205, doi:10.1029/2006JB004674.

Boudon, G., Villemant, B., Friant, A.L., Paterne, M. & Cortijo, E., 2013. Role of large flank-collapse events on magma evolution of volcanoes. Insights from the Lesser Antilles Arc., *J. Volc. Geotherm. Res.,* **263,** 224–237.

Briden, J.C., Rex, D.C., Faller, A.M. & Tomblin, J.F., 1979. K-Ar geochronology and paleomagnetism of volcanic-rocks in the lesser Antilles Island arc, *J. Volc. Geotherm. Res.,* **57,** 272–272.

Brown, M.C., Singer, B.S., Knudsen, M.F., Jicha, B.R., Finnes, E. & Feinberg, J.M., 2009. No evidence for Brunhes age excursions, Santo Antão, Cape Verde, *Earth planet. Sci. Lett.,* **287,** 100–115.

Calvo-Rathert, M., Reyes, B.A., Goguitchaichvili, A., Elguera, J.R., Franco, H., Morales, J. & Delgado, H., 2013. Rock-magnetic and paleomagnetic results from the Tepic-Zacoalco rift region (western Mexico), *Stud. Geophys. Geod.,* **57**(2), 309–331.

Cande, S.C. & Kent, D.V., 1995. Revised calibration of the geomagnetic polarity timescale for the Late Cretaceous and Cenozoic, *J. geophys. Res.: Solid Earth (1978–2012),* **100,** 6093–6095.

Carcaillet, J., Bourlès, D.L., Thouveny, N. & Arnold, M., 2004. A high resolution authigenic ^{10}Be/^{9}Be record of geomagnetic moment variations over the last 300 ka from sedimentary cores of the Portuguese margin, *Earth planet. Sci. Lett.,* **219,** 397–412.

Carlut, J. & Courtillot, V., 1998. How complex is the time-averaged geomagnetic field over the past 5 Myr, *Geophys. J. Int.,* **134,** 527–544.

Carlut, J., Quidelleur, X., Courtillot, V. & Boudon, G., 2000. Paleomagnetic directions and K/Ar dating of 0 to 1 Ma lava flows from La Guadeloupe Island (French West Indies): implications for time-averaged field models, *J. geophys. Res.: Solid Earth (1978–2012),* **105,** 835–849.

Ceja, M.R., Goguitchaichvili, A., Calvo-Rathert, M., Morales-Contreras, J., Alva-Valdivia, L., Elguera, J.R., Fucugauchi, J.U. & Granados, H.D., 2006. Paleomagnetism of the pleistocene tequila volcanic field (western Mexico), *Earth Planets Space,* **58,** 1349–1358.

Champion, D.E., Dalrymple, G.B. & Kuntz, M.A., 1981. Radiometric and paleomagnetic evidence for the Emperor reversed polarity event at 0.46 ± 0.05 My in basalt lava flows from the eastern Snake River Plain, Idaho, *Geophys. Res. Lett.,* **8,** 1055–1058.

Champion, D.E., Lanphere, M.A. & Kuntz, M.A., 1988. Evidence for a new geomagnetic reversal from lava flows in Idaho: discussion of short polarity reversals in the Brunhes and late Matuyama polarity chrons, *J. geophys. Res.: Solid Earth (1978–2012),* **93,** 11 667–11 680.

Channell, J., Hodell, D., Singer, B. & Xuan, C., 2010. Reconciling astrochronological and ^{40}Ar/^{39}Ar ages for the Matuyama-Brunhes boundary and late Matuyama Chron, *Geochem. Geophys. Geosyst.,* **11,** doi:10.1029/2010GC003203.

Coe, R.S., Jarboe, N.A., Le Goff, M. & Petersen, N., 2014. Demise of the rapid-field-change hypothesis at Steens Mountain: the crucial role of continuous thermal demagnetization, *Earth planet. Sci. Lett.,* **400,** 302–312.

Cogné, J., 2003. PaleoMac: a Macintosh^{TM} application for treating paleomagnetic data and making plate reconstructions, *Geochem. Geophys. Geosyst.,* **4,** doi:10.1029/2001GC000227.

Constable, C. & Parker, R., 1988. Statistics of the geomagnetic secular variation for the past 5 my, *J. geophys. Res.: Solid Earth (1978–2012),* **93,** 11 569–11 581.

Conte-Fasano, G., Urrutia-Fucugauchi, J., Goguitchaichvili, A. & Morales-Contreras, J., 2006. Low-latitude paleosecular variation and the time-averaged field during the late Pliocene and Quaternary: paleomagnetic study of the Michoacan-Guanajuato volcanic field, Central Mexico, *Earth, planets Space,* **58,** 1359–1371.

Cox, A., 1962. Analysis of present geomagnetic field for comparison with paleomagnetic results, *J. Geomagn. Geoelectr.,* **13,** 101–112.

Downloaded from http://gji.oxfordjournals.org/ at Erciyes University on December 21, 2014

Cox, A., 1969. Confidence limits for the precision parameter k, *J. Volc. Geotherm. Res.,* **17,** 545–549.

Creer, K., Readman, P. & Jacobs, A., 1980. Palaeomagnetic and palaeontological dating of a section at Gioia Tauro, Italy: identification of the Blake event, *Earth planet. Sci. Lett.,* **50,** 289–300.

Dunlop, D.J., 2002. Theory and application of the Day plot (Mrs/Ms versus Hcr/Hc) 1. Theoretical curves and tests using titanomagnetite data, *J. geophys. Res.: Solid Earth (1978–2012),* **107,** EPM 4-1–EPM 4-22.

Elmaleh, A., Valet, J.-P. & Herrero-Bervera, E., 2001. A map of the Pacific geomagnetic anomaly during the Brunhes chron, *Earth planet. Sci. Lett.,* **193,** 315–332.

Elmaleh, A. *et al.*, 2004. Palaeosecular variation in Java and Bawean Islands (Indonesia) during the Brunhes chron, *Geophys. J. Int.,* **157,** 441–454.

Fisher, R., 1953. Dispersion on a sphere, *Proc. R. Soc. Lond., Ser. A* **217,** 295–305.

Gee, J.S. & Kent, D.V., 2007. Source of oceanic magnetic anomalies and the geomagnetic polarity time scale, in *Treatise on Geophysics,* Vol. 5: Geomagnetism, pp. 455–507, ed. Kono, M., Elsevier.

Germa, A., Quidelleur, X., Labanieh, S., Lahitte, P. & Chauvel, C., 2010. The eruptive history of Morne Jacob volcano (Martinique Island, French West Indies): geochronology, geomorphology and geochemistry of the earliest volcanism in the recent Lesser Antilles arc., *J. Volc. Geotherm. Res.,* **198,** 297–310.

Germa, A., Quidelleur, X., Lahitte, P., Labanieh, S. & Chauvel, C., 2011. The K–Ar Cassignol–Gillot technique applied to western Martinique lavas: a record of Lesser Antilles arc activity from 2 Ma to Mount Pelée volcanism, *Quarter. Geochronol.,* **6,** 341–355.

Goguitchaichvili, M., Petronille, B., Henry & Alva-Valdivia, L., 2007. Paleomagnetism of Eastern Alkaline Province (southwestern Gulf of Mexico), *Earth Planets Space,* **59,** 775–784.

Gubbins, D., 1999. The distinction between geomagnetic excursions and reversals, *Geophys. J. Int.,* **137,** F1–F3.

Heller, F. & Petersen, N., 1982. Self-reversal explanation for the Laschamp Olby geomagnetic-field excursion, *Phys. Earth planet. Inter.,* **30,** 358–372.

Hoffman, K.A. & Singer, B.S., 2004. Regionally recurrent paleomagnetic transitional fields and mantle processes, *Geophys. Monogr. Ser.,* **145,** 233–243.

Johnson, C. *et al.*, 2008. Recent investigations of the 0–5 Ma geomagnetic field recorded by lava flows, *Geochem. Geophys. Geosyst.,* **9,** doi:10.1029/2007GC001696.

Kent, D.V., Wang, H. & Rochette, P., 2010. Equatorial paleosecular variation of the geomagnetic field from 0 to 3 Ma lavas from the Galapagos Islands, *Phys. Earth planet. Inter.,* **183,** 404–412.

Kidane, T. *et al.*, 2003. New paleomagnetic and geochronologic results from Ethiopian Afar: block rotations linked to rift overlap and propagation and determination of a ∼2 Ma reference pole for stable Africa, *J. geophys. Res.: Solid Earth (1978–2012),* **108,** doi:10.1029/2001JB000645.

Kirschvink, J., 1980. The least-squares line and plane and the analysis of palaeomagnetic data, *Geophys. J. Int.,* **62,** 699–718.

Krása, D., Shcherbakov, V.P., Kunzmann, T. & Petersen, N., 2005. Self-reversal of remanent magnetization in basalts due to partially oxidized titanomagnetites, *Geophys. J. Int.* **162,** 115–136.

Kruiver, P.P., Dekkers, M.J. & Heslop, D., 2001. Quantification of magnetic coercivity components by the analysis of acquisition curves of AF, *Earth planet. Sci. Lett.,* **189,** 269–276.

Lanphere, M.A., 2000. Comparison of conventional K–Ar and $^{40}Ar/^{39}Ar$ dating of young mafic volcanic rocks, *Quarter. Res.,* **53,** 294–301.

Lawrence, K.P., Constable, C.G. & Johnson, C.L. 2006. Paleosecular variation and the average geomagnetic field at ±20 latitude, *Geochem. Geophys. Geosyst.,* **7**(7), doi:10.1029/2005GC001181.

Le Friant, A., Ishizuka, O. & Stroncik, N.A.A. & the Expedition 340 Scientists, 2013. *Proceedings of the IODP,* Vol. 340, Tokyo (Integrated Ocean Drilling Program Management International, Inc.), doi:10.2204/iodp.proc.340.2013.

Le Goff, M. & Gallet, Y., 2004. A new three-axis vibrating sample magnetometer for continuous high-temperature magnetization measurements: applications to paleo- and archeo-intensity determinations, *Earth planet. Sci. Lett.* **229,** 31–43.

Lewis-Kenedi, C.B., Lange, R.A., Hall, C.M. & Delgado-Granados, H., 2005. The eruptive history of the Tequila volcanic field, western Mexico: ages, volumes, and relative proportions of lava types, *Bull. Volcanol.,* **67,** 391–414.

Lund, S., Stoner, J.S., Channell, J.E. & Acton, G., 2006. A summary of Brunhes paleomagnetic field variability recorded in Ocean Drilling Program cores, *Phys. Earth planet. Inter.,* **156,** 194–204.

MacLeod, C., Carlut, J., Escartín, J., Horen, H. & Morris, A., 2011. Quantitative constraint on footwall rotations at the 15° 45′ N oceanic core complex, Mid-Atlantic Ridge: implications for oceanic detachment fault processes, *Geochem. Geophys. Geosyst.,* **12,** doi:10.1029/2011GC003503.

McElhinny, M.W. & McFadden, P.L., 1997. Palaeosecular variation over the past 5 Myr based on a new generalized database, *Geophys. J. Int.,* **131,** 240–252.

McElhinny, M. & Merrill, R., 1975. Geomagnetic secular variation over the past 5 my, *Rev. Geophys.,* **13,** 687–708.

Mejia, V., Opdyke, N., Vilas, J., Singer, B. & Stoner, J., 2004. Plio-Pleistocene time-averaged field in southern Patagonia recorded in lava flows, *Geochem. Geophys. Geosyst.,* **5**(**3**), doi:10.1029/2003GC000633.

Mejia, V., Böhnel, H., Opdyke, N., Ortega-Rivera, M., Lee, J. & Aranda-Gomez, J., 2005. Paleosecular variation and time-averaged field recorded in late Pliocene–Holocene lava flows from Mexico, *Geochem. Geophys. Geosyst.,* **6,** doi:10.1029/2004GC000871.

Merrill, R.T. & McElhinny, M.W., 1977. Anomalies in the time-averaged paleomagnetic field and their implications for the lower mantle, *Rev. Geophys.,* **15,** 309–323.

Opdyke, N.D., Hall, M., Mejia, V., Huang, K. & Foster, D.A., 2006. Time-averaged field at the equator: results from Ecuador, *Geochem. Geophys. Geosyst.,* **7,** doi:10.1029/2005GC001221.

Opdyke, N.D., Kent, D.V., Huang, K.N., Foster, D.A. & Patel, J.P., 2010. Equatorial paleomagnetic time-averaged field results from 0–5 Ma lavas from Kenya and the latitudinal variation of angular dispersion, *Geochem. Geophys. Geosyst.,* **11,** doi:10.1029/2009GC002863.

Peña, R.M. *et al.*, 2009. Paleomagnetic and rock-magnetic survey of Brunhes lava flows from Tancitaro volcano, Mexico, *Geof. Int.,* **48**(4), 375–384.

Peña, R.M., Gogichaishvili, A., Guilbeaud, M.N., Ruiz Martinez, V., Siebe, C., Aguilar Reyes, B. & Morales, J., 2014. Paleomagnetic secular variation study of Ar–Ar dated lavas flows from Tacambaro Area (Central Mexico): possible evidence of Intra-Jaramillo geomagnetic excursion in volcanic rocks, *Phys. Earth planet. Inter.,* **229,** 98–109.

Petronille, M., Goguitchaichvili, A., Henry, B., Alva-Valdivia, L.M., Rosas-Elguera, J., Urrutia-Fucugauchi, J., Ceja, M.R. & Calvo-Rathert, M., 2005. Paleomagnetism of Ar-Ar dated lava flows from the Ceboruco-San Pedro volcanic field (western Mexico): evidence for the Matuyama-Brunhes transition precursor and a fully reversed geomagnetic event in the Brunhes chron, *J. geophys. Res.-Solid Earth,* **110,** doi:1029.2004JB003321.

Plenier, G., Valet, J.P., Guérin, G., Lefèvre, J.C., LeGoff, M. & Carter-Stiglitz, B., 2007. Origin and age of the directions recorded during the Laschamp event in the Chaîne des Puys (France), *Earth planet. Sci. Lett.,* **259**(3), 414–431.

Quidelleur, X. & Courtillot, V., 1996. On low-degree spherical harmonic models of paleosecular variation, *Phys. Earth planet. Inter.,* **95,** 55–77.

Quidelleur, X. & Valet, J.P., 1996. Geomagnetic changes across the last reversal recorded in lava flows: from La Palma, Canary Islands, *J. geophys. Res.-Solid Earth,* **101,** 13 755–13 773.

Quidelleur, X., Valet, J.P., Courtillot, V. & Hulot, G., 1994. Long-term geometry of the geomagnetic-field for the last 5 million years—an updates secular variation database, *Geophys. Res. Lett.,* **21,** 1639–1642.

Quidelleur, X., Gillot, P.-Y., Carlut, J. & Courtillot, V., 1999. Link between excursions and paleointensity inferred from abnormal field directions recorded at La Palma around 600 ka, *Earth planet. Sci. Lett.,* **168,** 233–242.

Quidelleur, X., Carlut, J., Tchilinguirian, P., Germa, A. & Gillot, P.-Y., 2009. Paleomagnetic directions from mid-latitude sites in the southern hemisphere (Argentina): contribution to time averaged field models, *Phys. Earth planet. Inter.,* **172,** 199–209.

Roberts, A., 2008. Geomagnetic excursions: knows and unknowns, *Geophys. Res. Lett.,* **35,** L17307, doi:10.1029/2008GL034719.

Downloaded from http://gji.oxfordjournals.org/ at Erciyes University on December 21, 2014

Samper, A., Quidelleur, X., Boudon, G., Le Friant, A. & Komorowski, J., 2008. Radiometric dating of three large volume flank collapses in the Lesser Antilles Arc, *J. Volc. Geotherm. Res.,* **176,** 485–492.

Sbarbori, E., Tauxe, L., Gogichaishvili, A., Urrutia, J. & Bohrson, W.A., 2009, Paleomagnetic behavior of volcanic rocks from Isla Socorro, Mexico, *Earth Planets Space,* **61,** 191–204.

Schneider, D.A. & Kent, D.V., 1990, The time-averaged paleomagnetic field, *Rev. Geophys.,* **28,** 71–96

Schnepp, E., 1996. Geomagnetic paleointensities derived from volcanic rocks of the Quaternary East Eifel volcanic field, Germany, *Phys. Earth planet. Inter.,* **94,** 23–41.

Singer, B., Relle, M., Hoffman, K., Battle, A., Laj, C., Guillou, H. & Carracedo, J., 2002. Ar/Ar ages from transitionally magnetized lavas on La Palma, Canary Islands, and the geomagnetic instability timescale, *J. geophys. Res.: Solid Earth (1978–2012),* **107,** EPM 7-1–EPM 7-20.

Singer, B.S., Hoffman, K.A., Schnepp, E. & Guillou, H., 2008. Multiple Brunhes Chron excursions recorded in the West Eifel (Germany) volcanics: support for long-held mantle control over the non-axial dipole field, *Phys. Earth planet. Inter.,* **169,** 28–40.

Tauxe, L. & Kent, D.V., 2004. A simplified statistical model for the geomagnetic field and the detection of shallow bias in paleomagnetic inclinations: was the ancient magnetic field dipolar?, in *Timescales of the Paleomagnetic Field,* pp. 101–116, eds Channell, J.E.T. *et al.*, Geophys. Monogr., 145.

Tauxe, L., Constable, C., Johnson, C.L., Koppers, A.A., Miller, W.R. & Staudigel, H., 2003. Paleomagnetism of the southwestern USA recorded by 0–5 Ma igneous rocks, *Geochem. Geophys. Geosyst.,* **4,** doi:10.1029/2002GC000343.

Tauxe, L., Luskin, C., Selkin, P., Gans, P. & Calvert, A., 2004. Paleomagnetic results from the Snake River Plain: contribution to the time-averaged field global database, *Geochem. Geophys. Geosyst.,* **5,** doi:10.1029/2003GC000661.

Udagawa, S., Kitagawa, H., Gudmundsson, A., Hiroi, O., Koyaguchi, T., Tanaka, H., Kristjansson, L. & Kono, M., 1999. Age and magnetism of lavas in Jökuldalur area, Eastern Iceland: Gilsá event revisited, *Phys. Earth planet. Inter.,* **115,** 147–171.

Valet, J.-P., Plenier, G. & Herrero-Bervera, E., 2008. Geomagnetic excursions reflect an aborted polarity state, *Earth planet. Sci. Lett.,* **274,** 472–478.

Valet, J.-P., Fournier, A., Courtillot, V. & Herrero-Bervera, E., 2012. Dynamical similarity of geomagnetic field reversals, *Nature,* **490,** 89–93.

Valet, J.-P. *et al.*, 2014. Geomagnetic, cosmogenic and climatic changes across the last geomagnetic reversal from Equatorial Indian Ocean sediments, *Earth planet. Sci. Lett.,* **397,** 67–79.

Watkins, N., 1973. Brunhes epoch geomagnetic secular variation on Reunion Island, *J. geophys. Res.,* **78,** 7763–7768.

Westercamp, D., Andreieff, P., Bouysse, P., Cottez, S. & Battistini, R., 1989. Notice explicative, *Carte géologique France à 1/50 000,* feuille Martinique, Orléans, BRGM, 246 pp.

Wilson, R., 1970. Permanent aspects of the Earth's non-dipole magnetic field over Upper Tertiary times, *Geophys. J. R. astr. Soc.,* **19,** 417–437.

Zanella, E., 1998. Paleomagnetism of Pleistocene volcanic rocks from Pantelleria Island (Sicily Channel), Italy, *Phys. Earth planet. Inter.,* **108,** 291–303.

SUPPORTING INFORMATION

Additional Supporting Information may be found in the online version of this article:

Figure S1. Hysteresis curves and parameters for all sites.
Figure S2. LogB1/2 and Dp parameters of the cumulative log-Gaussian function (Kruiver *et al.* 2001), various populations of Ti-Magnetite are in black (circle) and green (triangle) and hematite is in red (diamond).
Table S1. SIRM and CLG function parameters for all samples (http://gji.oxfordjournals.org/lookup/suppl/doi:10.1093/gji/ggu423/-/DC1).

Please note: Oxford University Press is not responsible for the content or functionality of any supporting materials supplied by the authors. Any queries (other than missing material) should be directed to the corresponding author for the article.

Downloaded from http://gji.oxfordjournals.org/ at Erciyes University on December 21, 2014